

## Order-parameter-fluctuation effects on the thermoelectric power above the superconducting transition in polycrystalline $\text{YBa}_2\text{Cu}_3\text{O}_{7-\delta}$

O. Cabeza, A. Pomar, A. Díaz, C. Torrón, J. A. Veira, J. Maza, and Félix Vidal  
*Laboratorio de Física de Materiales, Departamento de Física de la Materia Condensada,  
 Universidad de Santiago de Compostela, 15706, Spain*

(Received 8 June 1992)

This paper reports on detailed measurements of the thermoelectric power,  $S(T)$ , and of the electrical conductivity,  $\sigma(T)$ , in three polycrystalline  $\text{YBa}_2\text{Cu}_3\text{O}_{7-\delta}$  samples, all with almost the same composition ( $\delta \lesssim 0.10$ ) and single phase to within 4%, but with different granularity characteristics. The measurements were done in the temperature interval ranging from the superconducting transition ( $\sim 91$  K) to 300 K, and the temperature resolution was 50 mK for  $S(T)$  and 10 mK for  $\sigma(T)$ . Near the transition, the  $S(T)$  data are corrected from the effects associated with the nonzero temperature gradient ( $\nabla T \lesssim 1$  K  $\text{cm}^{-1}$ ) needed to perform the measurements. We also propose an empirical procedure to take into account the influence on  $S(T)$  of the structural inhomogeneities (grains, crystallites, twinings) at long length scales, i.e., at length scales much larger than the superconducting correlation length in all directions. From these  $S(T)$  and  $\sigma(T)$  data we extract, following consistent procedures, the corresponding excesses,  $\Delta S(\epsilon)$  and  $\Delta\sigma(\epsilon)$ , as a function of the reduced temperature,  $\epsilon$ . Our experimental data indicate that in the so-called mean-field-like region (MFR), i.e., between  $\epsilon \approx 5 \times 10^{-3}$  to  $\epsilon \approx 1.5 \times 10^{-1}$ , the reduced-temperature behavior of  $\Delta S(\epsilon)$  is not only very similar for the three different samples studied here, but also to that of  $\Delta\sigma(\epsilon)$ . In contrast, the amplitudes of  $\Delta S(\epsilon)$  and of  $\Delta\sigma(\epsilon)$  appreciably differ from sample to sample. When analyzed in terms of the empirical picture proposed here, that takes into account the influence on  $\Delta S(\epsilon)$  and on  $\Delta\sigma(\epsilon)$  of the structural inhomogeneities at long length scales, the above results strongly suggest that, at least within the MFR, all the critical behavior of  $S(\epsilon)$  near but above the transition in  $\text{YBa}_2\text{Cu}_3\text{O}_{7-\delta}$  samples is driven by that of  $\sigma(\epsilon)$ . These last results confirm, to a quantitative level, our earlier proposal that in single-crystal (in the  $ab$  plane) or in polycrystalline  $\text{YBa}_2\text{Cu}_3\text{O}_{7-\delta}$  compounds the thermoelectric power coefficient,  $L(\epsilon)$ , relating  $S(\epsilon)$  to  $\sigma(\epsilon)$ , is not affected, to within the measurements resolution, by the presence of superconducting-order-parameter fluctuations. The latter finding seems to be confirmed, at least at a qualitative level, by a recent theoretical calculation of  $\Delta L(\epsilon)$  in the MFR in layered superconductors.

### I. INTRODUCTION

Until the discovery of the high-temperature copper-oxide superconductors (HTSC), the influence of the thermodynamic fluctuations of the superconducting-order-parameter amplitude (OPF) on the thermoelectric power,  $S$ , in superconductors has remained as an interesting but mainly academic problem.<sup>1,2</sup> These effects could not be observed in bulk low-temperature metallic superconductors (LTS), mainly because their superconducting order-parameter correlation length amplitude,  $\xi(0)$ , was relatively important, typically of the order of 1000 Å. As a consequence, the temperature range over which one might expect to see OPF effects would be very small,<sup>1-3</sup> orders of magnitude less than the temperature differences needed to measure  $S$ . In the copper-oxide superconductors, however,  $\xi(0)$  is typically 2 orders of magnitude smaller than in LTS (so, the coherent volume in bulk samples is 6 orders of magnitude smaller) and the superconducting transition temperature is 1 order of magnitude higher, therefore, OPF effects will manifest themselves at easily accessible temperature distances from the superconducting transition. For instance, measurements of the electrical resistivity,  $\rho(T)$ , or of the magnetic susceptibility,  $\chi(T)$ , indicate that in HTSC the OPF effects

are appreciable even  $10^\circ$  above the superconducting transition.<sup>4-13</sup>

In spite of their interest and of the above-indicated experimental advantages, the OPF effects on  $S(T)$  above the superconducting transition in HTSC have been relatively little studied until now, and the emerging picture is rather confusing. For instance, in the case of single-crystal and polycrystalline  $\text{YBa}_2\text{Cu}_3\text{O}_{7-\delta}$  and related samples, most of the measurements indicate a relatively rounded peak of  $S(T)$  above the transition,<sup>14-20</sup> although in some works a very sharp peak of  $S(T)$  just above the transition has been observed.<sup>21,22</sup> Some authors have claimed that such a sharp peak is due to OPF effects,<sup>22</sup> although it could just be a spurious effect associated with sample temperature inhomogeneities.<sup>20</sup> The discrepancies concerning the OPF effects remain even amongst those papers that propose a qualitatively similar rounded  $S(T)$  peak above the transition. For instance, based on earlier normal-state theoretical works,<sup>14,21,23</sup> some authors propose that the OPF effects cause the  $S(T)$  rounded peak itself.<sup>17</sup> However, first Laurent and co-workers<sup>15,16,24</sup> and then Cabeza and co-workers,<sup>18,19,25</sup> taking into account that the measured  $S(T)$  strongly depends on the electrical resistivity, have proposed that the OPF effects probably cause the rounding of the  $S(T)$

peak above the transition, but not at all the peak itself, which will be associated with transport effects in the normal phase.<sup>26–32</sup> Nonetheless, important discrepancies still remain between the proposals of these last two groups in what concerns basic aspects of the OPF effects on  $S(T)$ . For example, Laurent and co-workers have proposed two- (2D) and four- (4D) dimensional OPF in  $\text{YBa}_2\text{Cu}_3\text{O}_{7-\delta}$  compounds,<sup>15,16</sup> and fractal dimensionality in Bi-based materials.<sup>16,24</sup> These proposals are not only in contrast with our results on the  $S(T)$  roundings,<sup>18,19,25</sup> but also with extensive work made in HTSC's on the electrical resistivity<sup>8,9</sup> and on the magnetic susceptibility<sup>10–13</sup> roundings above the transition, which clearly support the 3D and 2D nature of OPF in the mean-field region (MFR), i.e., from approximately 1 to 10 K from the transition for, respectively, Y-based and Bi-based superconductors.

The present discrepancies on the measured  $S(T)$  rounding above the superconducting transition in HTSC and on the conclusions about the corresponding OPF effects seem to be mainly associated with (i) the sensitivity of  $S(T)$  to compositional (in particular, oxygen content) or structural inhomogeneities at different length scales, from the interatomic distances (a few Å) to the characteristic lengths of the grains and crystallites in polycrystalline samples, or of the untwinned domains in single-crystal samples (typically, 1000 Å or higher),<sup>20,26–36</sup> (ii) the presence of spurious effects associated with temperature inhomogeneities induced during the  $S(T)$  measurements; and (iii) differences in the procedures followed to extract the OPF effects from  $S(T)$ . As a further contribution to the understanding of the OPF effects on  $S(T)$  in HTSC compounds, in this paper we present simultaneous measurements of the  $S(T)$  and  $\rho(T)$  roundings above the superconducting transition in three single-phase (to within 4%)  $\text{YBa}_2\text{Cu}_3\text{O}_{7-\delta}$  polycrystalline samples, all with the same nominal composition and with  $\delta \lesssim 0.10$ , but having a very distinct long length scale structural inhomogeneities. We propose, then, an empirical picture to account for the influence on  $S(T)$  of these structural inhomogeneities. The OPF effects on both magnitudes, extracted following consistent procedures, will be compared together and with the existing theories.

## II. EXPERIMENTAL DETAILS

### A. The samples

Three batches of granular  $\text{YBa}_2\text{Cu}_3\text{O}_{7-\delta}$  ceramic samples with  $\delta \lesssim 0.10$  were used. All the samples were prepared by usual solid-state synthesis procedure.<sup>37</sup> For the first batch of samples (noted Y1), constituent oxides, mixed in a stoichiometric ratio, were heated at 950°C for 24 h. The product was powdered, pelletized, and sintered at 900°C for 6 h in an oxygen atmosphere and then cooled to 200°C without cutting the oxygen flow. The material was maintained at this temperature for 2 h. For the second batch of samples (Y2), the constituent oxides, mixed in a stoichiometric ratio, were finally treated in air at 400°C for 7 d, followed by quenching in liquid nitrogen. The third batch of samples (Y3) was prepared in the

same way, except that the final product was slowly cooled down in air atmosphere.

All the samples are single phase within 4% as shown by x-ray analysis. Optical microscopy measurements and scanning electron microscopy (SEM) show that the typical grain and crystallite sizes of our polycrystalline samples are 1–20  $\mu\text{m}$ . The crystallites show also a high density of twin boundaries at a length scale larger than 1000 Å. The main structural difference between the various samples concerns the pores between the grains. In some of the samples these pores are relatively important, and they gave the same length scales as the grains and crystallites. This porosity reduces the sample average density to 80% of the ideal one, and also contributes to increase the normal resistivity by 1 or 2 orders of magnitude that of single crystals,  $\rho_{ab}$ . The average density of the less porous sample is of the order of 90% of the ideal one, and  $\rho(T)$  in the normal state is only a few times larger than  $\rho_{ab}(T)$ . In contrast with these important resistivity differences, the amplitude of  $S(T)$  for the different samples is always of the same order of magnitude as  $S_{ab}(T)$  in single crystals (see later).

### B. Experimental method and apparatus

We first recall that the absolute thermoelectric power  $S$  may be easily defined through  $\mathbf{J}_N$ , the number current density,<sup>38</sup>

$$-\mathbf{J}_N = \frac{\sigma}{e^2} \nabla \mu + \frac{\sigma S}{e} \nabla T, \quad (1)$$

where  $e$  is the carriers' electric charge,  $\sigma$  is the electrical conductivity,  $\nabla T$  is the temperature gradient, and

$$\mu = \mu_c + \mu_e, \quad (2)$$

where  $\mu_c$  is the chemical potential and  $\mu_e = -eV_e$ , with  $V_e$  being the ordinary electrostatic potential. To measure  $S$ , we employ the standard dc differential method under the condition  $\mathbf{J}_N = 0$ , which yields,<sup>39</sup>

$$\begin{aligned} \frac{\Delta V}{\Delta T} = & -\frac{1}{\Delta T} \int_{T-\Delta T/2}^{T+\Delta T/2} S(T') dT' \\ & + \frac{1}{\Delta T} \int_{T-\Delta T/2}^{T+\Delta T/2} S_{\text{leads}}(T') dT', \end{aligned} \quad (3)$$

where  $\Delta T$  and  $T$  are, respectively, the difference and the mean between both sample end temperatures, and  $\Delta V$  is the potential difference between leads (hot branch minus cold branch) measured at the voltmeter terminals. Since  $S_{\text{leads}}$  (in our case copper) is nonsingular at liquid- $\text{N}_2$  temperatures and above, one can approximate for moderate temperature differences

$$\begin{aligned} S_M(T) \equiv & \frac{1}{\Delta T} \int_{T-\Delta T/2}^{T+\Delta T/2} S(T') dT' \\ \approx & S_{\text{leads}}(T) - \frac{\Delta V}{\Delta T}, \end{aligned} \quad (4)$$

from which one can obtain the measured (average) thermopower,  $S_M$ , once  $S_{\text{leads}}$  is known. Note that  $\Delta V/\Delta T$  and, therefore,  $S_M(T)$  do not depend on the sample geometrical parameters. In other words, the determina-

tion of the absolute thermopower does not need the detailed knowledge of the sample geometry, in contrast with, for instance, the experimental determination of the sample electrical resistivity. We will see in Sec. III that this is an important advantage in the case of polycrystalline samples, where some undetermined porosity may be present.

The unavoidable use of a small but finite-temperature gradient to obtain the intrinsic thermopower,  $S(T)$ , is irrelevant when  $S(T)$  has a mild temperature dependence. However, such a temperature gradient may introduce spurious differences between  $S_M(T)$  and  $S(T)$  near the superconducting transition.<sup>15,23</sup> To obtain  $S(T)$  from  $S_M(T)$ , i.e., to eliminate the spurious effects generated near the transition by the finite-temperature gradient, we have used a numerical procedure. Essentially, this procedure consists in inverting Eq. (4) and recasting it into the form

$$S(T-n\Delta T) = S(T) - \Delta T \sum_{m=0}^{n-1} \frac{dS_M}{dT} \left[ T - \frac{\Delta T}{2} - m\Delta T \right], \quad (5)$$

where  $m$  and  $n$  are integers. This expression relates  $S(T)$  to  $S(T-n\Delta T)$  through the derivatives of the measured thermopower. Its application entails the following steps. First, we take  $T$  to be a fixed temperature well above the superconducting transition (say 110 K in our case) where one can neglect the nonzero temperature gradient effects on  $S(T)$ , i.e., where one can assume  $S(T) \approx S_M(T)$ . Then, the evaluation of the derivatives  $dS_M/dT$  at the discrete temperatures  $T - \Delta T/2 - m\Delta T$  ( $m = 1, 2, \dots, n-1$ ) yields directly  $S(T-n\Delta T)$ . Reconstruction of  $S(T)$  is accomplished by sweeping in  $n$ , so that  $T-n\Delta T$  spans in temperature the entire transition. Note that this procedure [from  $S_M(T)$  to  $S(T)$ ] is just the reversed one [from  $S(T)$  to  $S_M(T)$ ] reported by Laurent and co-workers in order to single out the effects of the  $\Delta T$ -induced spurious rounding.<sup>15</sup>

The samples, with typical size  $10 \times 2 \times 1$  mm<sup>3</sup>, were mounted on a specially designed sample holder assembly made up of copper. The schematic diagram of the low-temperature portion of the apparatus is shown in Fig. 1. As illustrated in this figure, the HTSC sample was fixed, symmetrically, between two microheaters with help of a spring arrangement. The main microheater was fixed

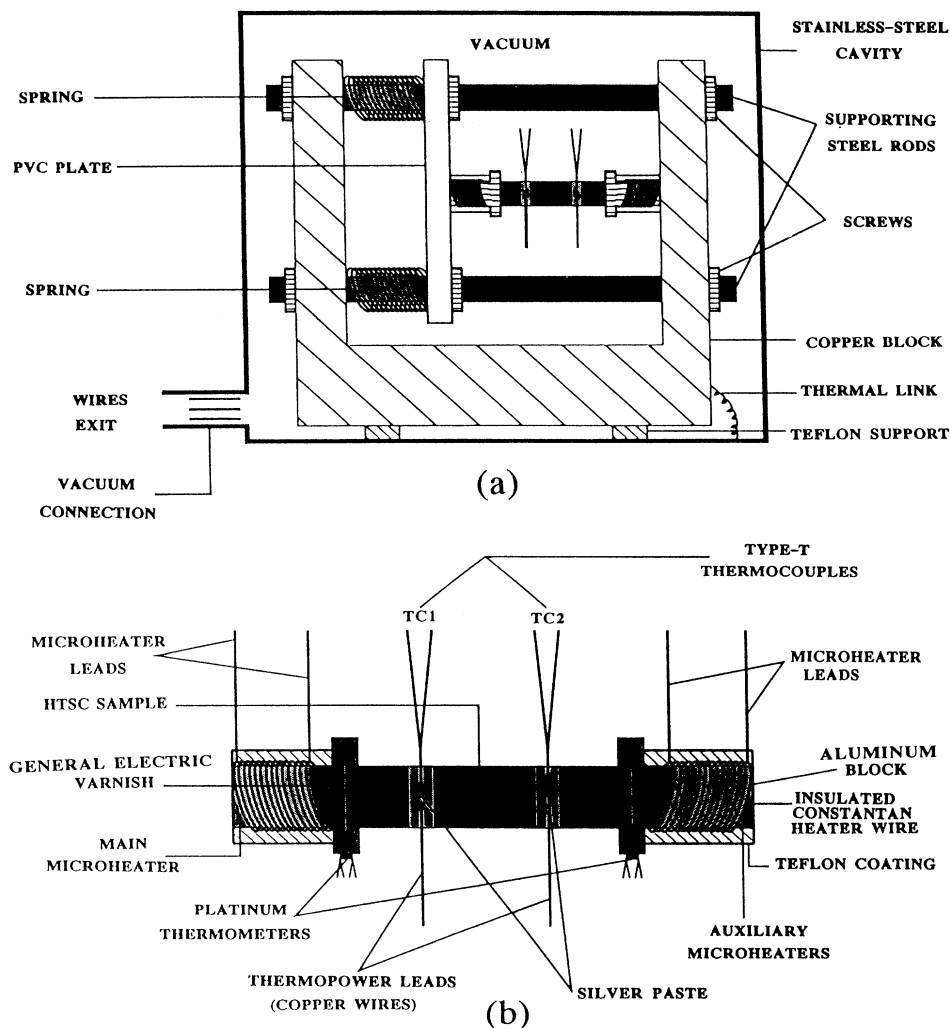


FIG. 1. Schematic diagram of the low-temperature portion of the experimental setup used to measure  $S(T)$  and  $\rho(T)$ . (a) General view. (b) Detail of the sample mounted for measurement.

with a isolated PVC plate, whereas the auxiliary microheater was fixed at a copper block. The sample holder assembly was placed in a stainless-steel cavity and the cavity was in contact with the cold tip of the cryostat. The microheaters were made by winding insulated constantan heater wire (diameter 0.1 mm) on small aluminum blocks and they were capable of giving several mW power. In order to avoid heat losses due, for instance, to radiation, the microheaters were embedded in teflon. General Electric Varnish 7031 was applied at both ends of the sample for better thermal contact with microheaters. The required temperature gradients across the sample was created by adjusting the current in the microheaters.

Two copper-constantan thermocouples (type  $T$ ), calibrated with a RhFe thermometer, were used to monitor the temperature gradient across the sample. As an average sample temperature, we use the half of the sum of the temperatures measured by these two thermocouples. Two platinum resistance thermometers were also used to control the sample end temperatures. A pair of copper leads (diameter 0.1 mm), attached to the sample with a minute amount of silver paste (Dupont 4929), were used to record the thermal voltage. The temperature difference was kept to within  $0.5\text{--}1\text{ K cm}^{-1}$  and we have checked that  $\Delta V/\Delta T$  is constant over that temperature gradient range. The temperature sweeping rate was about 5 K/h. An automated data acquisition system comprised of  $8\frac{1}{2}$  digits voltmeter with scanner and controller was used for data acquisition. Electrical resistivity of the samples was measured with a four-probe technique using the same data acquisition system as for  $S$ . Electrical resistivity and thermoelectric power resolutions were, respectively,  $1\mu\Omega\text{ cm}$  and  $0.1\mu\text{V K}^{-1}$ . Temperature resolution was 10 mK for  $\rho(T)$  and 50 mK for  $S(T)$ . Last, measured  $S$  data were corrected from the copper lead contribution,  $S_{\text{leads}}$  in Eq. (4), according to the standard tables.<sup>39</sup>

### III. EXPERIMENTAL RESULTS

#### A. Electrical resistivity

Although this paper is centered on the thermoelectric power, as noted before,  $S(T)$  is closely related to the electrical resistivity  $\rho(T)$ . So, in this section we will start by summarizing our results on  $\rho(T)$ . Figures 2(a) and 2(b) show the temperature dependence of the measured electrical resistivity of the three samples studied here. The most relevant general characteristics of these  $\rho(T)$  curves

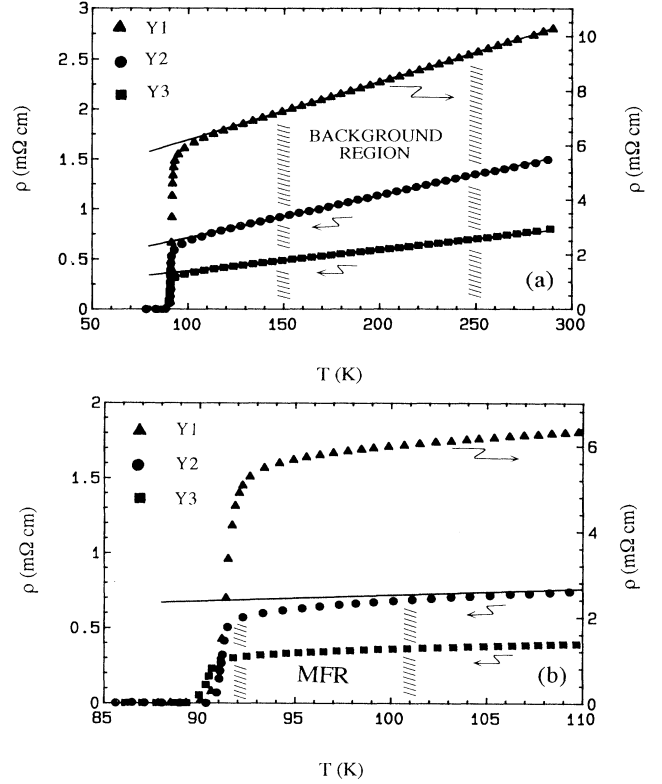


FIG. 2. Temperature behavior of the measured electrical resistivity of the three samples studied here. The solid lines represent the background resistivity fitted in the indicated region. (a) Over the entire temperature region measured. (b) Near the transition, showing the mean-field region (MFR) of sample Y2. Note that sample Y1 is scaled to the right axis in both figures.

are summarized in Table I. The notation is the same as in Refs. 8 and 9. In particular,  $d\rho/dT$  is the slope of  $\rho(T)$  between 150 and 250 K, a temperature range where  $\rho(T)$  may be fairly well approximated by a straight line with  $d\rho/dT > 0$ , i.e., where the resistivity of the three samples shows metallic behavior.  $T_c$  is defined by  $\rho(T_c) = 0$ , to within the measurement resolution.  $T_{CI}$  is the temperature where  $\rho(T)$  around the transition has its inflexion point, and  $\Delta T_{CI}$  is the upper half-width of the resistive transition<sup>8</sup> (see later). Note that, whereas  $T_c$  will be appreciably affected by the granular nature of our

TABLE I. General electrical resistivity ( $\rho$ ) characteristics of the samples.  $T_c$  is the upper temperature where  $\rho(T) = 0$ ,  $T_{CI}$  is the temperature where  $\rho(T)$  has its inflexion point,  $\Delta T_{CI}$  is the upper half-width of the resistive transition, and  $p$  and  $\rho_{ct}$  are coefficients associated to the sample polycrystallinity. The meaning of the other parameters is evident.

Sample	$\rho$ (300 K) ( $m\Omega\text{ cm}$ )	$T_c$ (K)	$T_{CI}$ (K)	$\rho(T_{CI})$ ( $m\Omega\text{ cm}$ )	$\Delta T_{CI}$ (K)	$(d\rho/dT)_{T > 150\text{ K}}$ ( $\mu\Omega\text{ cm K}^{-1}$ )	$p$ ( $10^2$ )	$\rho_{ct}$ ( $\mu\Omega\text{ cm}$ )
Y1	10.5	89.6	91.3	2.3	0.4	21.5	2.0	53
Y2	1.56	90.6	91.1	0.3	0.3	4.2	11.9	36
Y3	0.81	89.5	90.5	0.2	0.2	2.1	22.7	39

samples,  $T_{CI}$  is expected to be close to the mean-field-like normal-superconducting transition temperature of the grains.<sup>8,9,12,40</sup> So, the differences in  $T_{CI}$  for the various samples in Table I are probably due to small differences in their oxygen content. Much more important are the differences in their normal dc resistivity,  $\rho(300\text{K})$ , or in the temperature slope of  $\rho(T)$  in the normal region far away from  $T_{CI}$ . These last differences may be easily explained in terms of a phenomenological picture, similar to that first proposed by Kirtley and co-workers for granular low-temperature superconductors,<sup>41</sup> that takes into account the presence in our granular samples of *structural* inhomogeneities at length scales much bigger than any characteristic length relevant for OPF as, for instance, the superconducting correlation length in all directions,  $\xi(T)$ , the effective interplane ( $\text{CuO}_2$ ) distances,  $d_e$ , or the electrical carriers mean free path,  $l$ .<sup>8,9</sup> In this picture, above  $T_{CI}$  each crystallite is supposed then to behave as a (random oriented) single crystal. The measured resistivity above  $T_{CI}$  and in zero applied magnetic field,  $\rho(T)$ , is related to the intrinsic resistivity in the  $ab$  plane of an ideal single crystal,  $\rho_{ab}$ , by<sup>8,40</sup>

$$\rho(T) = \frac{1}{p} [\rho_{ab}(T) + \rho_{ct}] . \quad (6)$$

The fact that  $\rho(T)$  depends only on  $\rho_{ab}(T)$  is because the resistivity in the  $c$  direction is orders of magnitude larger than in the  $ab$  plane.<sup>6,7</sup> In Eq. (6),  $p$  ( $0 < p \leq 1$ ) is associated both with a reduction of the cross-section area of the sample, due, for instance, to sample porosity, and with a path lengthening due to the random orientation of the  $ab$  planes of the different grains or twinning domains.  $\rho_{ct}$  is an average resistivity that accounts for the contact resistance between different long-scale sample domains (grains, untwinned domains, etc.). The differences in  $p$  in Table I are, therefore, mainly correlated, as indicated before, with sample porosity differences. The way we have rewritten Eq. (6) (compare with the equivalent expression in Refs. 8 and 40) is to emphasize the fact that the inter-grain electric contact resistances of the three samples studied here must be relatively similar. This qualitative conclusion is in good agreement with the  $\rho_{ct}$  values of Table I. Indeed,  $\rho_{ct}$  below  $T_{CI}$  must become temperature dependent, in order to get  $\rho(T_c) = 0$ . In that case, Eq. (6) clearly shows the distinct nature of  $T_c$  and  $T_{CI}$  in granular samples: whereas  $T_{CI}$  concerns only the term  $\rho_{ab}(T)$  associated with the grains,  $T_c$  concerns  $\rho_{ct}(T)$ .

The coefficients arising in the measured electrical resistivity and associated with the sample polycrystallinity,  $p$  and  $\rho_{ct}$ , are extracted for each sample by comparing its normal resistivity far away from the transition ( $150 \leq T \leq 250$  K), to avoid the presence of critical phenomena,<sup>8</sup> with the resistivity in the  $ab$  plane of a single crystal ( $p \approx 1$ ,  $\rho_{ct} \approx 0$ ) of the same composition. The available  $\rho_{ab}(T)$  data in different single crystals are well fitted, in this *background* region, by<sup>6,7,42</sup>

$$\rho_{abB}(T) = C_1 + C_2 T , \quad (7)$$

with  $C_1 = (5 \pm 15) \mu\Omega \text{ cm}$ , and  $C_2 = (0.5 \pm 0.2) \mu\Omega \text{ cm K}^{-1}$ , which corresponds to the average values from the data of

Refs. 6, 7, and 42. We note that in some cases, in particular for polycrystalline YBCO samples with oxygen deficiencies bigger than  $\delta = 0.15$ , the normal resistivity is much better fitted (always in the same background temperature region) if a  $1/T$  contribution is added in Eq. (7).<sup>43</sup> Such a “semiconductor” behavior has been earlier proposed by Anderson and Zou<sup>44</sup> to take into account the scattering mechanism in the transport between  $ab$  planes. However, recent measurements in fully oxygenated single YBCO crystals show that even  $\rho_c$  (the resistivity in the  $c$  direction) has an almost linear temperature dependence<sup>7</sup> and, therefore, the  $1/T$  contribution is probably, in the case of these samples, nonintrinsic. It must be stressed, anyhow, that the precise functional form of  $\rho_{abB}(T)$  has a relatively small influence on the extraction of the critical contributions.<sup>8,9,40</sup> This is because when analyzing critical phenomena, the precise choice of the background should be of small relevance provided that a high-quality fitting in a wide  $T$  region is realized and also that the extrapolation through the transition is smooth.<sup>45</sup>

In Figs. 3(a) and 3(b) we present the  $\rho_{ab}(T)$  curves extracted from the  $\rho(T)$  data given in Figs. 2(a) and 2(b) by

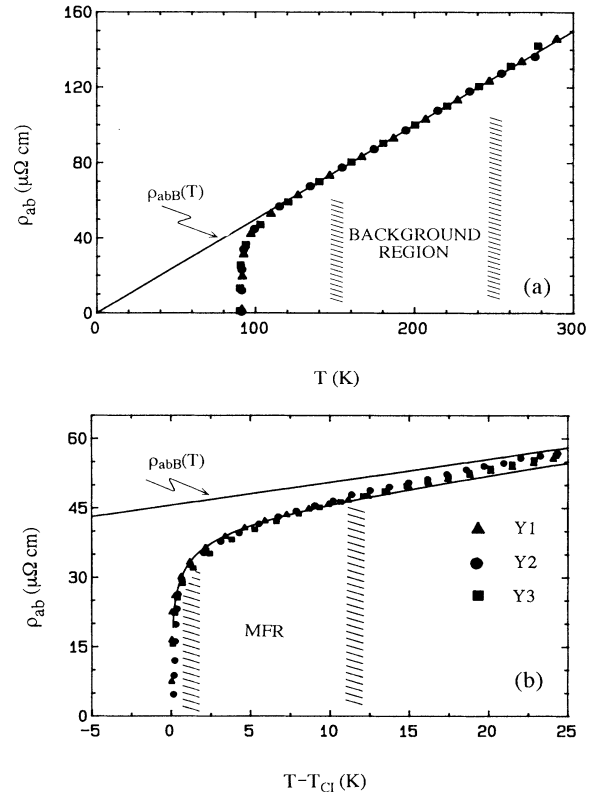


FIG. 3. Temperature behavior of the intrinsic electrical resistivity, extracted from the measured resistivity for each sample used here. The coefficients for the intrinsic background are,  $C_1 = 0$  and  $C_2 = 0.5 \mu\Omega \text{ cm K}$ . (a) General view. (b) Near the transition, showing the average mean-field region (MFR) for the three samples. The solid line through the points is the best fit of the Lawrence-Doniach approach, Eq. (41). See main text for details.

using Eqs. (6) and (7), the corresponding  $p$  and  $\rho_{ct}$  values being those given in Table I and with  $C_1=0$  and  $C_2=0.5\mu\Omega\text{ cm K}^{-1}$ . As expected, the  $\rho(T)$  measurements in the three single-phase samples having the same nominal composition but very different long-scale structural inhomogeneities lead, to within the experimental uncertainties, to the same  $\rho_{ab}(T)$  values, which also coincide with those measured in the best single-crystal samples<sup>6,7,42</sup> over the whole temperature range above  $T_{CI}$ . So, the dramatic differences for the paraconductivity in the  $ab$  plane,  $\Delta\sigma_{ab}(\epsilon)$ , among some of these works,<sup>7,42</sup> with one on one side and our results on the other, are just due to differences in the extraction of  $\Delta\sigma_{ab}(\epsilon)$  from the same  $\rho_{ab}(T)$  curve. These differences, which have been described in Ref. 9, are mainly associated with the arbitrary use, in some of these works, of a free background and a free mean-field critical temperature,  $T_{C0}$  (see later).

### B. Thermoelectric power

Figures 4(a) and 4(b) show the temperature dependence of the thermoelectric power in the zero temperature gradient limit,  $S(T)$ , for the same three samples as the  $\rho(T)$  curves in Figs. 2(a) and 2(b) (with similar, but open, data

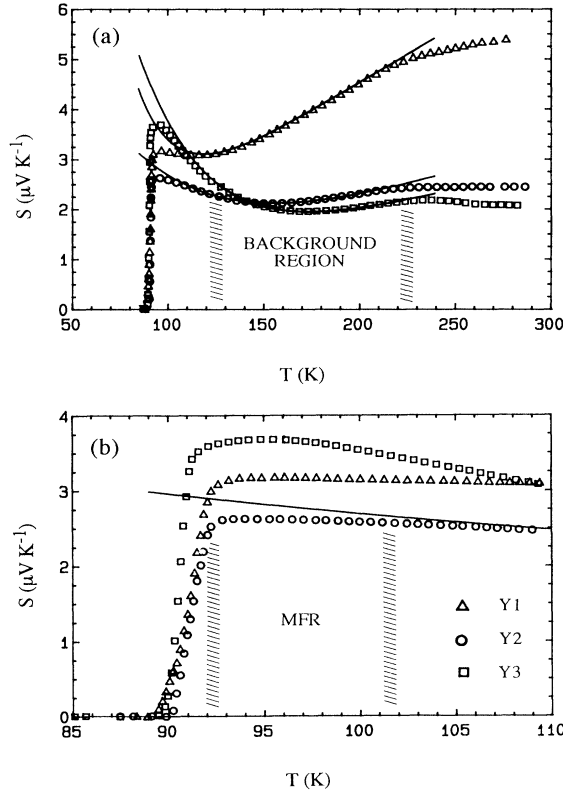


FIG. 4. Temperature behavior of the thermoelectric power of the three samples used here. The solid lines represent the  $S(T)$  background, fitted in the indicated region. (a) Over the entire temperature region measured. (b) Near the transition, showing the mean-field region (MFR) of sample Y2.

symbols).  $S(T)$  has been obtained from the measured  $S_M(T)$  following the numerical procedure described in Sec. II B. An example of the influence of the nonzero temperature gradient on the measured thermoelectric power near the transition is given in Fig. 5. This figure corresponds to sample Y2 and to a temperature difference between the sample ends of  $\Delta T=2$  K. We see, therefore, that even for a relatively important  $\Delta T$  (in most of our measurements  $\Delta T \lesssim 1$  K) the corresponding corrections on  $S_M(T)$  are relatively small and, more importantly, do not almost affect  $S(T)$  in the MFR. However,  $\Delta T$  changes also slightly the temperature where  $S(T)$  has its inflexion point, noted  $T_{CI}^S$ , which we are going to use as the mean-field-like temperature for  $S(T)$  (see later). These corrections, already introduced in the curves of Fig. 4(b), must therefore be taken into account to extract the OPF influence on the measured thermoelectric power.

The main general characteristics of the  $S(T)$  curves in Figs. 4(a) and 4(b) are summarized in Table II. In particular, and in analogy with Table I for  $\rho(T)$ ,  $S(300\text{ K})$  is the extrapolated thermopower amplitude at 300 K,  $T_C^S$  is the temperature where  $S(T)$  becomes nonmeasurable,  $T_{CI}^S$  is the temperature where  $S(T)$  near the transition has its inflexion point,  $S(T_{CI}^S)$  is the thermopower amplitude at  $T_{CI}^S$ , and  $\Delta T_{CI}^S$  is the upper half-width of the thermopower transition and it is defined by

$$\left. \frac{dS(T)}{dT} \right|_{T_{CI}^S + \Delta T_{CI}^S} = \frac{1}{2} \left. \frac{dS(T)}{dT} \right|_{T_{CI}^S}. \quad (8)$$

The last four columns in Table II concern some thermopower background characteristics and they will be defined and commented on later.

The data presented in Fig. 4 indicate that the  $S(T)$  amplitudes of the three samples studied here differ with each other by less than a factor of 3 over all the temperature regions studied. These amplitude differences still

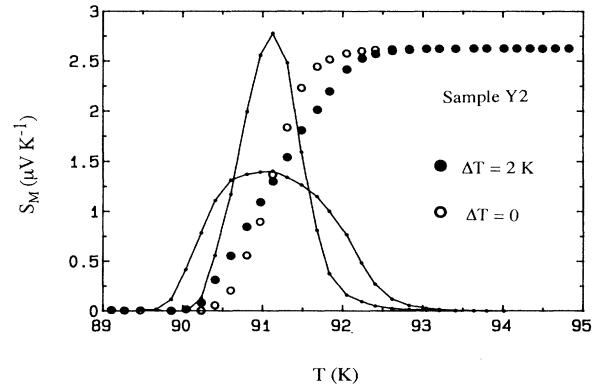


FIG. 5. Example of the influence of the nonzero temperature gradient on the measured thermoelectric power. The solid symbols represent the measured thermopower,  $S_M(T)$ , and the open symbols have been extracted from these data by eliminating the spurious effects due to the finite-temperature gradient used during the measurement. See main text for details.

TABLE II. General thermoelectric power ( $S$ ) characteristics of the samples.  $T_C^S$  is the temperature where  $S(T)$  becomes nonmeasurable,  $T_{CI}^S$  is the temperature where  $S(T)$  near the transition has its inflexion point,  $\Delta T_{CI}^S$  is the upper half-width of the thermopower transition, and the parameters  $a$ ,  $b$ , and  $T_0$  correspond to the background function,  $S_B(T)$ . The meaning of the other parameters is evident.

Sample	$S$ (300 K) ( $\mu$ V K $^{-1}$ )	$T_C^S$ (K)	$T_{CI}^S$ (K)	$S(T_{CI}^S)$ ( $\mu$ V K $^{-1}$ )	$\Delta T_{CI}^S$ (K)	$S_B(T_{CI}^S)$ ( $\mu$ V K $^{-1}$ )	$a$ ( $10^2 \mu$ V K $^{-2}$ )	$b$	$T_0$ (K)
Y1	4.8	89.3	91.3	1.9	0.5	3.8	2.26	260	16.0
Y2	2.2	89.9	91.1	1.2	0.4	2.9	1.09	35	31.4
Y3	2.1	89.8	90.6	2.1	0.5	4.5	0.95	140	25.9

remain relatively small when compared with  $S_{ab}(T)$ , the thermoelectric power in the  $ab$  plane measured in single-crystal samples of similar chemical composition.<sup>26–32</sup> This is in contrast with the much more important differences for the resistivity amplitudes corresponding to the same samples, as observed in Fig. 2, mainly when compared with  $\rho_{ab}(T)$  (Fig. 3). These qualitative results clearly confirm that  $S(T)$  is much less sensitive than  $\rho(T)$  to the long-scale structural inhomogeneities.<sup>20,26–36,43</sup> This is mainly due to the fact that, as noted in Sec. II,  $S(T)$  is an intensive magnitude (unlike the electrical resistance), but also because in  $\text{YBa}_2\text{Cu}_3\text{O}_{7-\delta}$  samples the intrinsic thermopower amplitude is much less anisotropic than the intrinsic resistivity amplitude,<sup>26–29</sup> so the effects of the random orientation of the  $ab$  planes in polycrystal samples are less important for  $S(T)$ .

In contrast with the results for the measured amplitudes, the results of Figs. 2 and 4 also indicate that the *temperature behavior* of  $S(T)$  differs much more than that of  $\rho(T)$  from sample to sample. In the case of  $\rho(T)$ , we have already seen that all the curves in the normal region well above the transition may be approximated by a straight line, only the slopes and the constant terms being variable from sample to sample. These results seem to be due to the fact that, in contrast with resistivity, thermopower is very sensitive to short length structural or compositional (oxygen content) inhomogeneities, at interatomic scales.<sup>20,26–36</sup> Note also that the broad peak of  $S(T)$  centered on about 230 K is also characteristic of  $\text{YBa}_2\text{Cu}_3\text{O}_{7-\delta}$  compounds, and have been observed by numerous authors,<sup>8–11,15,21,24,27</sup> but its physical origin is not yet totally clear. Some authors suggest that it may be due to a phonon-drag effect.<sup>15</sup> However, other authors relate it with the possible antiferromagnetic transition of the YBCO compounds around that temperature. This transition would originate magnetic excitations, producing then an extra contribution to the thermopower (the so-called magnon-drag thermopower).<sup>27</sup> Finally, the results for  $T_{CI}^S$  and  $T_C^S$  in Tables I and II show that, in each sample, both transition temperatures differ by less than 0.1 K, i.e., these differences are well to within  $\Delta T_{CI}^S$  or  $\Delta T_C^S$ . This last result is illustrated in Fig. 6 for the Y2 sample.

In analogy with Eq. (6) for  $\rho(T)$ , it will be useful to phenomenologically explain the above results for  $S(T)$  by introducing an empirical relation between the measured thermopower in *single-phase* granular samples,  $S(T)$ , with the intrinsic thermopower in the  $ab$  plane,  $S_{ab}(T)$ , in

an ideal single crystal of the same nominal composition. For that purpose, we may assume first that in measuring  $S$ , an intensive magnitude, the random distribution of the  $ab$  planes and  $c$  directions of the grains, crystallites, and untwinned domains in a polycrystalline sample is equivalent to a sample having  $ab$  and  $c$  paths in parallel. So, by applying Eq. (1) under the condition  $\mathbf{J}_N=0$ , the *equivalent* thermopower,  $S^e$ , is easily found to be<sup>46</sup>

$$S^e = \frac{S_{ab}\sigma_{ab} + S_c\sigma_c}{\sigma_{ab} + \sigma_c} \approx S_{ab},$$

where we have assumed  $\sigma_{ab} \gg \sigma_c$ ,<sup>6,7</sup> whereas  $S_{ab}$  and  $S_c$  are of the same order of magnitude in  $\text{YBa}_2\text{Cu}_3\text{O}_{7-\delta}$  samples.<sup>26,29</sup> Now, the differences between  $S$  and  $S^e$  are due to the presence in the real granular sample of intergrains and interfaces having some effective thermal resistivity and thermopower. We may thus suppose that only a fraction,  $p^s\Delta T$  of the temperature difference  $\Delta T$  used to measure  $S$  drops within the intragains, the other fraction,  $(1-p^s)\Delta T$ , being associated with the intergrains and interfaces. Therefore,  $S(T)$  may be crudely related to  $S_{ab}(T)$  by

$$S(T) = p^s S_{ab}(T) + S_{ct}(T), \quad (9)$$

where  $p^s$  ( $0 < p^s \leq 1$ ) is the coefficient that takes into account the relative gradient temperature distribution between intragains and intergrains,  $S_{ct} \equiv (1-p^s)S_{ct}^e$  will be the contribution to  $S(T)$  associated with the sample interdomains (grains, crystallites, untwinned regions), and

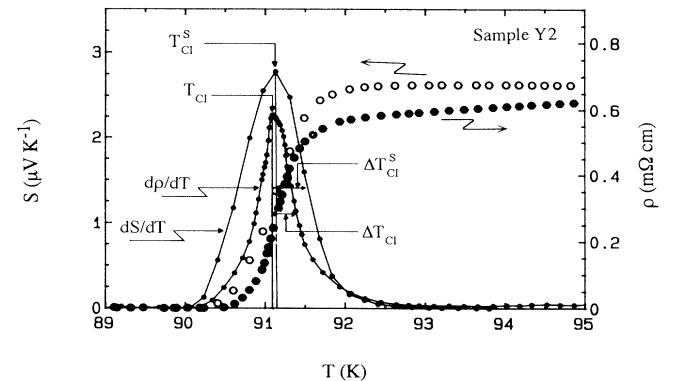


FIG. 6. Resistivity  $\rho(T)$  and thermopower  $S(T)$  of sample Y2 around the superconducting transition.

$S_{ct}^e$  is the “effective” thermopower of these sample interfaces. The possible presence of small inhomogeneities (structural or compositional) at short length scales will also arise through  $S_{ct}^e$ .

Note that  $p^s$  will depend on  $S_{ct}^e(T)$  and on the intragrain and intergrain thermal conductivities and, therefore,  $p^s$  will have a weak  $T$  dependence. For  $T < T_{CI}^S$ ,  $S_{ct}$  must vanish. On the other side, to take into account that  $T_{CI}^S (\approx T_{CI})$  is almost the same for the different samples having the same nominal composition, one must assume  $dS_{ct}(T)/dT \ll dS_{ab}(T)/dT$  near but above the transition. So whereas the amplitude differences between  $S(T)$  and  $S_{ab}(T)$  will be due to both  $p^s$  and  $S_{ct}(T)$ , variations in the temperature behavior will be mainly associated with  $S_{ct}(T)$ . We will see in Sec. IV that the decomposition of  $S(T)$  indicated by Eq. (9), although somewhat arbitrary, is very useful to describe some qualitative aspects of the OPF influence on  $S(T)$ . Equation (9) is also useful to describe an important difference between  $\rho(T)$  and  $S(T)$ : As indicated in Sec. III B, it is possible to extract the whole  $\rho_{ab}(T)$  curve for  $T > T_{CI}$  from the  $\rho(T)$  data if  $\rho_{ab}(T)$  is known in the normal (background) region. This is because  $p$  and  $\rho_{ct}$  in Eq. (6) are temperature independent, but it is not the case of  $S_{ct}$  in Eq. (9), which will have an unknown temperature dependence. We thus cannot extract  $S_{ab}(T)$  from our data in granular samples. Another qualitative difference between  $\rho(T)$  and  $S(T)$  will arise through  $p$  and  $p^s$ : As  $S(T)$  is an intensive magnitude,  $p^s$  in Eq. (9) is expected to vary from sample to sample much less than  $p$  in Eq. (6) because  $S(T)$  will not be, as noted before and unlike the measured sample resistance,  $R(T)$ , sensitive to the reduction of the effective sample section, caused, for instance, by sample porosity.

Let us now introduce a possible functional form for  $S(T)$  in the normal region, far away from the transition (to avoid the presence of critical phenomena) as it will be used as *background* in the extraction of the excess thermopower (see next section). Amongst the various possible functional forms for the thermopower background,  $S_B(T)$ , for Y-based compounds, we have chosen that proposed in Ref. 47,

$$S_B(T) = aT(1 + be^{-T/T_0}), \quad (10)$$

where  $a$ ,  $b$ , and  $T_0$  are free parameters. We do not claim this functional form to represent better than other the physics of thermopower of the YBCO system in the normal state, but, as indicated before for  $\rho_B(T)$ , Eq. (10) gives a high-quality fitting in a wide  $T$  region well above the transition. As our previous  $\rho(T)$  results strongly suggest that the OPF effects in  $YBa_2Cu_3O_{7-\delta}$  compounds are not appreciable above 120 K,<sup>8,9,12,40,48</sup> Eq. (10) has been fitted to the measured  $S(T)$  over the temperature interval 120–220 K. Note that by approaching the background region to the transition it is possible to better take into account the rounded peak near  $T_{CI}^S$  associated with transport effects in the normal phase. As can be seen in Fig. 4(a), the fit quality is excellent, the rms being for the three samples less than 4%, including the experimental errors. The corresponding  $a$ ,  $b$ , and  $T_0$  values are given in Table II. Note, finally, that Eq. (10) will correspond to

the measured thermopower background in our polycrystalline samples. This is in contrast with the resistive background for our samples, which is obtained from  $\rho_{abB}(T)$  of an ideal single crystal [Eq. (7)] through Eq. (6). In the case of thermopower, the relationship between  $S(T)$  and  $S_{ab}(T)$  [Eq. (9)] contains the unknown temperature-dependent term,  $S_{ct}(T)$ , and a possible expression for  $S_{abB}(T)$  cannot be directly used to analyze our samples.

## IV. DATA ANALYSIS

### A. General aspects

To analyze the rounding effects of  $S(T)$  and  $\sigma(T)$  above the superconducting transition observed in Figs. 2–6 and, in particular, to compare these effects with the existing theoretical approaches on the influence of the order-parameter fluctuations on these quantities, we must introduce the measured excess thermoelectric power,  $\Delta S(\epsilon)$ , and the measured excess electrical conductivity (the so-called paraconductivity),  $\Delta\sigma(\epsilon)$ , defined by

$$\Delta S(\epsilon) \equiv S_B(\epsilon) - S(\epsilon) \quad (11)$$

and

$$\Delta\sigma(\epsilon) \equiv \sigma(\epsilon) - \sigma_B(\epsilon), \quad (12)$$

where  $S(\epsilon)$  or  $\sigma(\epsilon)$  and, respectively,  $S_B(\epsilon)$  or  $\sigma_B(\epsilon)$  correspond to the measured and background magnitudes defined in the foregoing section. Here  $\epsilon$  is the reduced temperature defined as

$$\epsilon \equiv \ln \frac{T}{T_{CI}^S} \approx \frac{T - T_{CI}^S}{T_{CI}^S} \quad (13)$$

in the case of  $\Delta S(\epsilon)$ , and as

$$\epsilon \equiv \ln \frac{T}{T_{CI}} \approx \frac{T - T_{CI}}{T_{CI}} \quad (14)$$

in the case of  $\Delta\sigma(\epsilon)$ . Note that for each sample both reduced temperatures are, as expected, very close to each other (see Tables I and II), the small differences being due to experimental uncertainties and spurious effects.

In Figs. 7 and 8 we show two different representations of both measured excesses.  $\Delta S(\epsilon)$  has been obtained by using in Eq. (11) the  $S(T)$  data of Figs. 4(a) and 4(b), and with  $S_B(T)$  obtained from Eq. (10), with the values of Table II for the corresponding free parameters.  $\Delta\sigma(\epsilon)$  has been obtained by using in Eq. (12) the  $\rho(T)$  data of Figs. 2(a) and 2(b), and with  $\sigma_B(T) [\equiv 1/\rho_B(T)]$  obtained directly by linearly extrapolating through the transition the measured  $\rho(T)$  in the normal region above 150 K.

Before comparing  $\Delta\sigma(\epsilon)$  and  $\Delta S(\epsilon)$  with each other, we must already stress here that Figs. 7 and 8 show two important and complementary results: (i) The amplitude of  $\Delta S(\epsilon)$  and, independently, of  $\Delta\sigma(\epsilon)$  varies from sample to sample. (ii) The  $\log_{10}\epsilon$  behavior of  $\Delta\sigma(\epsilon)$  and, independently, of  $\Delta S(\epsilon)$  is, to within the experimental uncertainties, similar for the three different samples over all

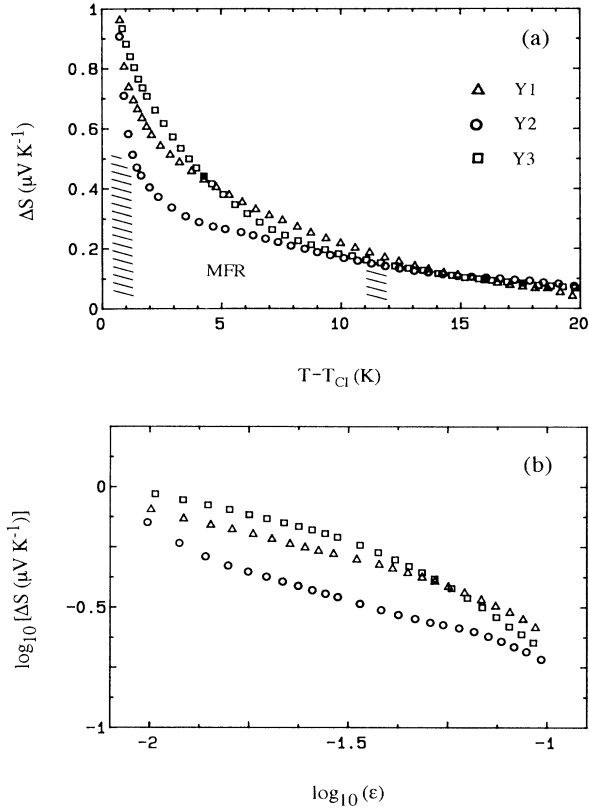


FIG. 7. Excess thermoelectric power vs reduced temperature for the three samples used here. (a)  $\Delta S$  vs  $T - T_{CI}^S$ . The average mean-field (MFR) for the three samples is indicated. (b) log-log plot.

the temperature ranges examined. These results clearly suggest that the presence of structural inhomogeneities at long length scales modifies the measured excess amplitudes of both observables, mainly in the case of  $\Delta\sigma(\epsilon)$ , but has a negligible influence on their temperature behavior. In the case of paraconductivity these results for *single-phase* polycrystalline samples were first presented in Ref. 48 and explained on the grounds of Eq. (6) in Ref. 8. Before analyzing the corresponding results for  $\Delta S(\epsilon)$ , let us summarize here the phenomenological explanation for  $\Delta\sigma(\epsilon)$ .

By applying Eq. (6) to the background region, we obtain

$$\rho_B(T) = \frac{1}{p} [\rho_{abB}(T) + \rho_{ct}], \quad (15)$$

where  $\rho_B(T)$  is the measured background (normal) resistivity of a polycrystalline sample and  $\rho_{abB}(T)$  is the background resistivity in the *ab* plane of an ideal single crystal of the same composition. By combining Eqs. (6), (12), and (15), we obtain

$$\Delta\sigma(\epsilon) = \frac{p}{F(\epsilon)} \Delta\sigma_{ab}(\epsilon), \quad (16)$$

where

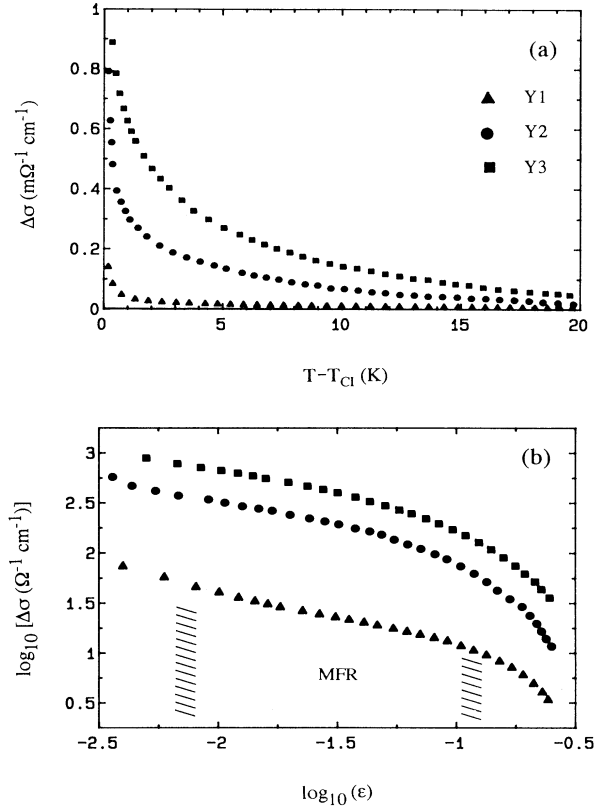


FIG. 8. Excess conductivity (paraconductivity) vs reduced temperature for our samples. (a)  $\Delta\sigma$  vs  $T - T_{CI}$ . (b) log-log plot. The average mean-field region (MFR) for the three samples is indicated.

$$F(\epsilon) \equiv \frac{\rho(\epsilon)\rho_B(\epsilon)}{[\rho(\epsilon) - \rho_{ct}/p][\rho_B(\epsilon) - \rho_{ct}/p]} \quad (17)$$

and

$$\Delta\sigma_{ab}(\epsilon) = \sigma_{ab}(\epsilon) - \sigma_{abB}(\epsilon) \quad (18)$$

is the paraconductivity in the *ab* plane of the ideal single crystal. Over the entire mean-field region, i.e., approximately between  $T_{CI} + 1$  K and  $T_{CI} + 11$  K (see later),  $F(\epsilon)$  will change very slowly as a function of  $\epsilon$  and, therefore, it may be approximated as a constant. For instance, over the above indicated temperature interval, in the case of sample Y1,  $2.9 \lesssim F(\epsilon) \lesssim 3.5$  whereas  $3.1 \lesssim F(\epsilon) \lesssim 4.0$  for sample Y3. So, Eq. (16) fully explains the above-indicated results for  $\Delta\sigma(\epsilon)$ . In particular, from Eq. (16) we have

$$\log_{10}\Delta\sigma(\epsilon) = \log_{10}\frac{p}{F} + \log_{10}\Delta\sigma_{ab}(\epsilon), \quad (19)$$

where the first term on the right-hand side of this equation is sample dependent but almost temperature independent, in full agreement with the results shown by Fig. 8(b). So, concerning  $\Delta\sigma(\epsilon)$  in the MFR, Eq. (16) indicates that, in agreement with experimental results, (i) the *reduced temperature dependence* of  $\Delta\sigma(\epsilon)$  in all

single-phase granular samples of the same composition must be similar to each other and also similar to that of a single-crystal sample in the  $ab$  plane; (ii) in contrast, the amplitude of the measured excess conductivity will be  $p/F$  times that of the corresponding single-crystal sample. Finally, for completeness we present in Figs. 9(a) and 9(b) two representations of  $\Delta\sigma_{ab}(\epsilon)$  extracted from the  $\rho(T)$  data of Figs. 2(a) and 2(b) by using Eq. (16). Indeed, the same results may be obtained directly from the data points of Figs. 3(a) and 3(b) by using Eq. (18).

The results of Figs. 7(a) and 7(b) for  $\Delta S(T)$  summarized before may also be explained on the ground of the empirical picture introduced in Sec. III. By applying Eq. (9) to the background (normal) region, we obtain

$$S_B(T) = p^s S_{abB}(T) + S_{ct}(T), \quad (20)$$

where  $S_B(T)$  is the measured background thermopower of a polycrystalline sample and  $S_{abB}(T)$  is the background thermopower in the  $ab$  plane of an ideal single crystal of the same composition. By combining Eqs. (9), (11), and (20), we obtain

$$\Delta S(\epsilon) = p^s \Delta S_{ab}(\epsilon), \quad (21)$$

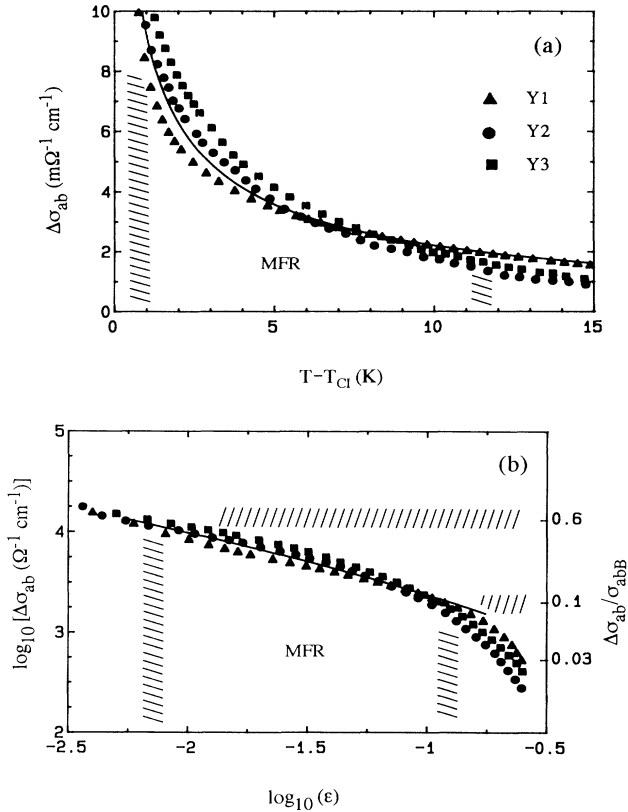


FIG. 9. Intrinsic paraconductivity vs reduced temperature extracted from the three samples used here. The solid line is the best fit of the Lawrence-Doniach approach in the indicated mean-field region (MFR). (a)  $\Delta\sigma_{ab}$  vs  $T - T_{Ct}$ . (b) log-log plot. The  $\Delta\sigma_{ab}/\sigma_{abB}$  limits of the average mean-field region (MFR) for the three samples are also indicated.

where

$$\Delta S_{ab}(\epsilon) \equiv S_{abB}(\epsilon) - S_{ab}(\epsilon) \quad (22)$$

is the thermopower excess of the ideal single crystal in the  $ab$  plane. We see, therefore, that  $\Delta S(\epsilon)$  and  $\Delta S_{ab}(\epsilon)$  are related through a sample-dependent, but almost temperature-independent parameter,  $p^s$ . Also, due to the intensive character of thermopower,  $p^s$  will change relatively little from sample to sample [in contrast with the parameter  $p$  associated with  $\Delta\sigma(\epsilon)$ ]. The amplitude of  $\Delta S(T)$  will thus change moderately from sample to sample. These results from Eq. (21) are in agreement with the experimental findings illustrated by Figs. 7(a) and 7(b).

An important difference when analyzing  $\Delta\sigma(\epsilon)$  and  $\Delta S(\epsilon)$  in polycrystalline samples, already noted in the foregoing section for  $\rho(T)$  and  $S(T)$ , is associated with the distinct behavior of  $\rho_{ct}$  and  $S_{ct}(T)$  in, respectively, Eqs. (6) and (9). In the expression relating  $\rho(T)$  to  $\rho_{ab}(T)$ , both  $p$  and  $\rho_{ct}$  are temperature-independent parameters and, therefore, they may be easily obtained by comparing  $\rho_B(T)$  with the available  $\rho_{abB}(T)$  in the background (normal) region:  $p$  is directly related to  $d\rho_B/dT$ , whereas  $\rho_{ct}$  is related to the  $\rho_B(T)$  amplitude. In fact,  $\rho_{ct}$  may be approximated as  $p\rho(T_{Ct})$ ,<sup>8</sup> and the knowledge of  $d\rho_{abB}/dT$  will suffice to determine  $\rho_{ab}(T)$  from  $\rho(T)$  over the entire temperature range above  $T_{Ct}$ . The situation is more complicated in the case of  $S(T)$  because  $S_{ct}(T)$  is, as noted before, temperature dependent. So,  $p^s$  and  $S_{ct}(T)$  cannot be disentangled by comparing  $S_B(T)$  with the available  $S_{abB}(T)$  data.  $p^s$  could be estimated only if  $S_{ab}(T)$  in a single-crystal sample with identical chemical composition is known. However, we must stress that the results of Fig. 7(b) confirm, to within the experimental uncertainties, the correctness of Eq. (21), and also show, when compared with Fig. 8(b), that  $p^s$  changes much less from sample to sample than  $p$ . Furthermore, Eq. (21) suggests that the reduced temperature behavior of  $\log_{10}\Delta S(\epsilon)$  in Fig. 7(b) will be close to that of  $\log_{10}\Delta S_{ab}(\epsilon)$ .

## B. Thermoelectric excess versus paraconductivity

As it is well known from irreversible thermodynamics, for small temperature gradients the (measured) thermoelectric power and the (measured) electrical resistivity are linearly related through the so-called thermopower coefficient,  $L(T)$ , which may be defined as<sup>38</sup>

$$L(T) \equiv S(T)\sigma(T). \quad (23)$$

We will assume here that this very general result, independent of any detailed model, applies for HTSC over all the region above the superconducting transition, even in the presence of OPF effects. The basic question is then how  $L(T)$  above, but near the transition, is affected by OPF. The natural and direct way to answer this question is to proceed as in the case of  $S(T)$  and  $\sigma(T)$ , i.e., to introduce the (measured) background thermopower coefficient,  $L_B(T)$ , by

$$L_B(T) \equiv S_B(T)\sigma_B(T), \quad (24)$$

where  $S_B(T)$  and  $\sigma_B(T)$  are the background magnitudes defined in the foregoing section.  $L_B(T)$  is then the thermopower coefficient near the transition but in the absence of OPF effects. From Eqs. (23) and (24), we may define the (measured) thermopower coefficient excess,  $\Delta L(T)$ , as

$$\Delta L(T) \equiv L(T) - L_B(T) = S(T)\sigma(T) - S_B(T)\sigma_B(T). \quad (25)$$

The next step will be to relate  $\Delta L(T)$  to  $\Delta S(T)$ . This can be directly done by using the definitions of  $\Delta S$  and  $\Delta\sigma$  given by Eqs. (11) and (12), to obtain

$$\Delta L(\epsilon) = S_B(\epsilon)\Delta\sigma(\epsilon) - \sigma(\epsilon)\Delta S(\epsilon), \quad (26)$$

which can be rewritten as

$$\frac{\Delta L(\epsilon)}{L_B(\epsilon)} = \frac{\Delta\sigma(\epsilon)}{\sigma_B(\epsilon)} - \frac{\sigma(\epsilon)}{\sigma_B(\epsilon)} \frac{\Delta S(\epsilon)}{S_B(\epsilon)}, \quad (27)$$

where, by convenience, we have used  $\epsilon$  instead of the absolute temperature. Let us stress that these expressions for  $\Delta L(\epsilon)$  are very general and do not depend on any particular model for the excesses of the three quantities involved,  $S(\epsilon)$ ,  $\sigma(\epsilon)$ , and  $L(\epsilon)$ . Equations (23)–(27) concern, as noted already, the *measured* magnitudes. However, the same procedure applied to the magnitudes for the *ab* plane of an ideal single crystal leads to

$$\begin{aligned} \Delta L_{ab}(\epsilon) &\equiv L_{ab}(\epsilon) - L_{abB}(\epsilon) \\ &= S_{abB}\Delta\sigma_{ab}(\epsilon) - \sigma_{ab}(\epsilon)\Delta S_{ab}(\epsilon), \end{aligned} \quad (28)$$

which may be seen as the limit of Eq. (26) to the ideal single-crystal case.

In Figs. 10(a)–10(c), we plot the two contributions to  $\Delta L/L_B$  in Eq. (27),  $\Delta\sigma/\sigma_B$  and  $(\sigma/\sigma_B)\Delta S/S_B$ , as a function of  $\log_{10}\epsilon$ . For the three polycrystalline samples studied here, having similar composition but different granularity, both terms have very similar amplitude and reduced-temperature behavior, over all the  $\epsilon$  range examined. Therefore, as shown also in these figures,  $\Delta L(\epsilon)$ , the corresponding thermopower coefficient excess, is temperature independent, and it has a very small negative amplitude which may be approximated as zero to within the experimental uncertainties. Note that the  $\epsilon$  range studied here spans all of the MFR. As this result is found for three samples having different structural inhomogeneities at large length scales, it seems that we may conclude that such a behavior is intrinsic to  $\text{YBa}_2\text{Cu}_3\text{O}_{7-\delta}$  samples, and also that  $\Delta L_{ab}(\epsilon) \approx 0$ . In other words, these results fully confirm at a quantitative level our previous experimental findings for YBCO (Refs. 18 and 19) or Bi-based samples,<sup>19</sup> and strongly suggest that the critical behavior observed for  $S(\epsilon)$  in the MFR will be essentially due to  $\sigma(\epsilon)$ . The thermopower coefficient,  $L$ , of YBCO samples above the superconducting transition will not be, to within the experimental uncertainties, affected by OPF.

In addition to the intrinsic interest in analyzing the OPF influence on the HTSC properties above but near the superconducting transition (see also next subsection),

the result  $\Delta L(\epsilon) \approx 0$  also has interesting implications for  $S(\epsilon)$  or  $L(\epsilon)$  over the entire region where  $\Delta S(\epsilon) \neq 0$ . By imposing  $\Delta L(\epsilon) = 0$  [and then  $\Delta L_{ab}(\epsilon) = 0$ ] in Eqs. (26) and (28), and using Eqs. (6), (15)–(17), and (21), it is easy to obtain

$$L(T) = p^s p L_{ab}(T), \quad (29)$$

and from Eqs. (6), (9), (23), and (29)

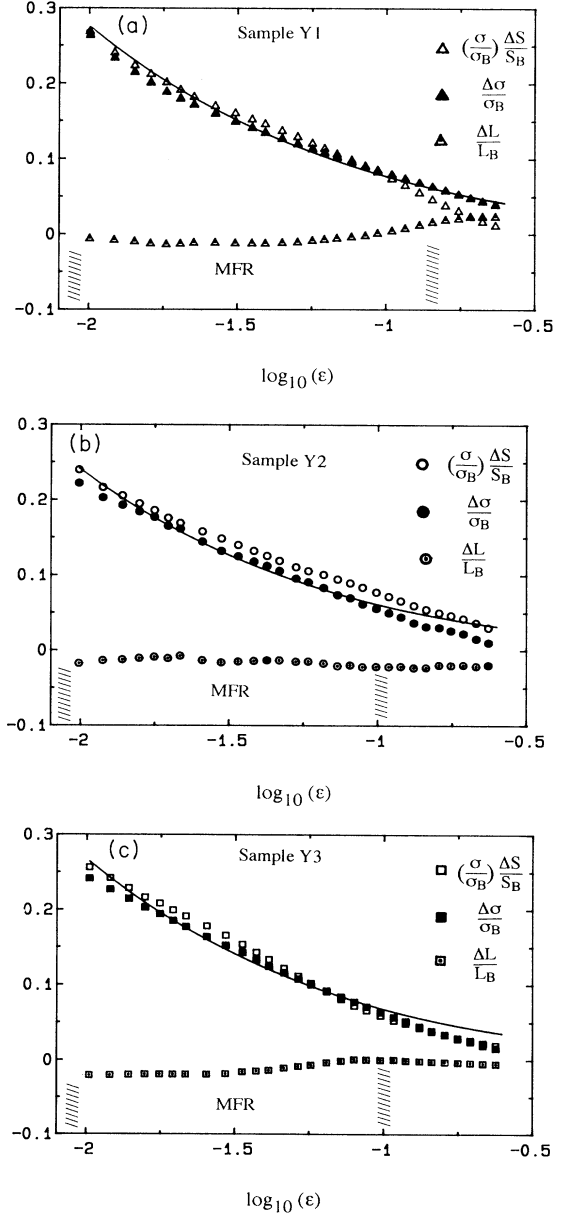


FIG. 10. Normalized excess of  $S(T)$  (open symbols),  $\sigma(T)$  (solid symbols), and  $L(T)$  (dotted symbols) vs the logarithm of the reduced temperature for, respectively, samples (a) Y1, (b) Y2, and (c) Y3. In each figure, the solid line is the best fit of the LD approach to the normalized paraconductivities in the indicated mean-field region (MFR).

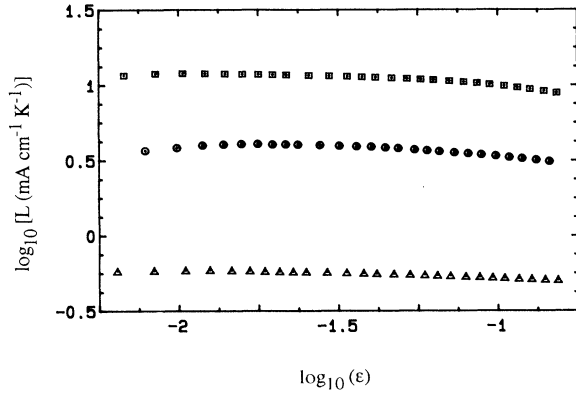


FIG. 11. log-log plot of the thermoelectric coefficient,  $L(T)$ , near the superconducting transition vs reduced temperature for the three samples studied here.

$$S_{ct}(T) = \frac{\rho_{ct}}{p} L(T). \quad (30)$$

These expressions being, indeed, applicable near the transition, in the region where  $\Delta S \neq 0$  and  $\Delta\sigma \neq 0$ . In addition, we must note that probably both expressions are more severely affected by the various simplifying approximations involved in our empirical pictures of  $\rho(T)$  and  $S(T)$ , due to the condition  $\Delta L(\epsilon) = 0$  used in their deduction. However, they may serve to check, at least qualitatively, these pictures. In particular, Eq. (29) predicts that, near the transition, the  $\epsilon$  dependence of the thermoelectric coefficient will be the same for all the samples with similar composition, independently of their long-scale structural inhomogeneities. This prediction is fairly well confirmed by the experimental results of  $L(T)$  presented in Fig. 11. These data correspond to the three YBCO samples studied in this work. Furthermore, the results of Fig. 11 show important differences in the amplitude of  $L$  for the various samples, much more important than those of  $\Delta S(T)$  [see Fig. 7(b)]. These amplitude differences may also be easily understood at a qualitative level by comparing Eqs. (21) and (29): in the case of  $L$ , the amplitude differences are mainly associated with those of  $p$ , which varies much more than  $p^5$  from sample to sample [see Table I for  $p$ ; the relative  $p^5$  from sample to sample may be qualitatively deduced from Fig. 7(b)].

### C. Comparison with other experimental results on $\Delta S$ and $\Delta L$

The differences and similarities of our results to other authors' involve, of course, the following main ingredients: original  $S(T)$  data, background function choice, and excess analysis. We are going to comment briefly here on the analyses and results from the only three groups known to us that have studied experimentally OPF effects in single-crystal and polycrystal  $\text{YBa}_2\text{Cu}_3\text{O}_{7-\delta}$  compounds.<sup>15–17,22</sup> As the data are concerned, Houson and co-workers<sup>22</sup> obtain  $S_{ab}(T)$  curves that present the anomalous steep peak at the superconducting transition alluded to in the Introduction. So, their results on  $\Delta L$  are not comparable with ours. How-

ever, such a peak has not been yet reproduced, and it could be just a spurious effect.<sup>19,20</sup> Moreover, we have checked that our  $S(T)$  data are very similar to theirs, once that peak is removed, as well as to the other two groups.

In what concerns the background function used to obtain  $\Delta S$  from  $S(T)$ , the discrepancies amongst these groups increase. In the case of Dey and co-workers,<sup>17</sup> they chose an  $S_B(T)$  so that their  $S(T)$  data, including the characteristic rounded peak, lie above  $S_B(T)$ . In our opinion there are two main drawbacks in their  $\Delta S$  extraction. First, it leads to the existence of an appreciable (negative)  $\Delta S$  even at  $T - T_C^S \approx 60$  K, although different measurements of  $\Delta\sigma$  (Refs. 8 and 9) or of  $\Delta\chi$  (Refs. 10–13) clearly indicate that the OPF effects are negligible so far from the transition [see, for instance, Fig. 2(a)]. Second, the analysis of these authors entails the attribution of the characteristic rounded peak in  $S(T)$  to OPF effects, in spite of the fact that it is commonly interpreted as normal-state transport effects.<sup>29–32</sup> The background function used by Salamon's group<sup>22</sup> seems unrealistic to us since they use a temperature-independent background, which is taken to be  $S(T)$  at  $T = 100$  K.

Regarding excess analysis, the main difference comes with Ausloos and co-workers.<sup>15,16</sup> Essentially these last authors seek the critical exponents on  $d\Delta S(T)/dT$  and  $d\Delta\rho(T)/dT$ , instead of on  $\Delta S$  and  $\Delta\sigma$  directly. It is not difficult to see that the critical exponents of  $d\Delta\rho(T)/dT$  are those of  $\Delta\sigma$  (the quantity for which theoretical predictions are available), only as long as the  $\epsilon$  dependence of  $\sigma$  over the MFR is neglected, which is contradictory in itself. On the other hand, we have seen that the pertinent quantity for theoretical comparison is  $\sigma\Delta S$  rather than  $\Delta S$  itself (see Sec. IV B and Refs. 18 and 19).

## V. COMPARISON WITH THE THEORETICAL APPROACHES

### A. Reduced-temperature location of the MFR

The comparison between our experimental data on  $\Delta S(T)$  and  $\Delta\sigma(T)$  and the existing theoretical approaches will be centered here on the so-called mean-field region, i.e., in the reduced-temperature range where the time-dependent Ginzburg-Landau- (TDGL) like approaches and the Gaussian approximations for OPF in zero applied magnetic field are expected to be applicable. As our previous results have suggested,<sup>8,9,12,49</sup> the reduced-temperature location of the MFR may approximately be bounded through the relative paraconductivity amplitude as<sup>49</sup>

$$0.1 \lesssim \frac{\Delta\sigma_{ab}(\epsilon)}{\sigma_{abB}(\epsilon)} \lesssim 0.6, \quad (31)$$

which, in the case of the YBCO samples studied here, will correspond, as indicated in Fig. 9(b), to  $7 \times 10^{-3} \lesssim \epsilon \lesssim 1.3 \times 10^{-1}$ . Here  $\epsilon$  is defined by Eq. (14), with the mean-field-like critical temperature being approximated by  $T_{CI}$  (see later). The lower  $\epsilon$  limit is associated with the so-called Ginzburg reduced temperature,

$\epsilon_G$ , which for OPF in three dimensions, the case which is expected to hold in the case of the  $\text{YBa}_2\text{Cu}_3\text{O}_{7-\delta}$  superconductors,<sup>8,9,12</sup> is given by<sup>50</sup>

$$\epsilon_G = \frac{1}{32\pi^2} \left[ \frac{k_B}{\xi_{ab}^2(0)\xi_c(0)\Delta C} \right]^2, \quad (32)$$

where  $k_B$  is the Boltzmann constant,  $\xi_{ab}(0)$  and  $\xi_c(0)$  are the order-parameter correlation length amplitudes in the  $ab$  plane and, respectively, in the  $c$  direction (normal to these superconducting  $ab$  planes), and  $\Delta C$  is the specific-heat jump at the transition. For the  $\text{YBa}_2\text{Cu}_3\text{O}_{7-\delta}$  samples, the values of these parameters proposed in the literature are<sup>51,52</sup> (see also later)

$$\begin{aligned} \xi_{ab}(0) &= (12 \pm 3) \text{ \AA}, \\ \xi_c(0) &= (2 \pm 1) \text{ \AA}, \end{aligned} \quad (33)$$

and<sup>52</sup>

$$\Delta C \approx 5 \times 10^4 \text{ J m}^{-3} \text{ K}^{-1}, \quad (34)$$

and, therefore, from Eq. (32) we obtain

$$\epsilon_G \approx 6 \times 10^{-3},$$

in excellent agreement with the lower  $\epsilon$  limit given by Eq. (31). Above the high-temperature limit bounded by Eq. (31), not only will the slow variation condition of the TDGL-like theories probably fail,<sup>53,54</sup> but also any calculation of the OPF effects cannot be trusted unless it takes full account of the dynamic local effects.<sup>3,53-55</sup> In addition, by using the accepted  $\epsilon$  dependence of the order-parameter correlation lengths in the MFR,

$$\xi_c(\epsilon) = \xi_c(0)\epsilon^{-1/2} \quad (35)$$

and  $\xi_c(0) = 1.5 \text{ \AA}$ , we see that for  $\epsilon \gtrsim 0.15$ ,  $\xi(\epsilon) \lesssim 3.9 \text{ \AA}$ , this length being close to the distance between the closest adjacent  $\text{CuO}_2$  planes in  $\text{YBa}_2\text{Cu}_3\text{O}_{7-\delta}$  samples ( $3.4 \text{ \AA}$ ). Therefore, for  $\epsilon \gtrsim 0.15$  the conventional approaches for single-layered superconductors are probably no longer applicable (see below). For still higher reduced-temperature ranges,  $\xi_c(\epsilon)$  will become even smaller than the interatomic distances. Notice that in the case of  $\Delta\sigma(\epsilon)$  and of the paramagnetism, the corresponding upper half-width of the transition,  $\Delta T_{CI}$  or  $\Delta T_{C\chi}$ , is less than  $T_G - T_{CI}$  or  $T_G - T_{C\chi}$  (see Table I). Therefore, we have probably been able to probe the so-called crossover and critical regions beyond the MFR, closer to the superconducting transition.<sup>9,12,56</sup> Although so close to the transition the critical exponents of both  $\Delta\sigma_{ab}(\epsilon)$  and  $\Delta\chi_{ab}(\epsilon)$  strongly depend on the precise choice of the transition temperature, our experimental results are fairly well *compatible* with the predictions of the scaling approaches.<sup>9,12,56</sup>

In the case of  $S(\epsilon)$ , due to the temperature gradients needed to perform the measurements, it is not possible to obtain  $\Delta S(\epsilon)$  for  $\epsilon \lesssim 0.01$ , i.e., for this observable we cannot penetrate beyond the MFR, closer to the transition. It is interesting, however, to obtain the reduced temperature location of the MFR in terms of  $\Delta S(T)/S_B(T)$ , as was done by Eq. (31) in terms of  $\Delta\sigma_{ab}(\epsilon)/\sigma_{abB}(\epsilon)$ . By

imposing our previous experimental finding,

$$\Delta L_{ab} \approx 0, \quad (36)$$

in Eq. (28), we obtain

$$\frac{\Delta S_{ab}(\epsilon)}{S_{abB}(\epsilon)} \approx \frac{\sigma_{abB}(\epsilon)}{\sigma_{ab}(\epsilon)} \frac{\Delta\sigma_{ab}(\epsilon)}{\sigma_{abB}(\epsilon)}, \quad (37)$$

and, therefore, Eq. (31) may be rewritten as

$$0.1 \lesssim \frac{\Delta S_{ab}(\epsilon)}{S_{abB}(\epsilon)} \lesssim 0.45, \quad (38)$$

where we have already used the experimental values  $\sigma_{abB}(\epsilon)/\sigma_{ab}(\epsilon) \approx 0.76$  or  $0.95$  for, respectively,  $\epsilon = 7 \times 10^{-3}$  or  $\epsilon = 0.13$ , for  $\text{YBa}_2\text{Cu}_3\text{O}_{7-\delta}$  compounds. Although we do not have access to  $\Delta S_{ab}(\epsilon)$  from our measurements in polycrystal samples [in contrast with  $\Delta\sigma_{abB}(\epsilon)$ , see Sec. III], by using Eqs. (20), (21), and (30), we have in the MFR,

$$\frac{\Delta S_{ab}(\epsilon)}{S_{abB}(\epsilon)} \approx \frac{\Delta S(\epsilon)}{S_B(\epsilon) - (\rho_{ct}/p)L}, \quad (39)$$

and, therefore, Eq. (38) may be rewritten as

$$0.1 \lesssim \frac{\Delta S(\epsilon)}{S_B(\epsilon) - (\rho_{ct}/p)L} \lesssim 0.45. \quad (40)$$

By using for  $\Delta S(\epsilon)$  the results of Fig. 7(a), the values deduced from Eq. (10) with the  $a$ ,  $b$ , and  $T_0$  values of Table II for  $S_B(\epsilon)$ , the values of Fig. 11 for  $L$ , and the values of Table I for  $\rho_{ct}$ , we obtain for the *three distinct samples* studied here,  $\epsilon \approx 8 \times 10^{-3}$ , for the low reduced-temperature limit of the MFR, whereas  $\epsilon \approx 0.12$  for the high reduced-temperature limit. The qualitative agreement of these values with those deduced from Eq. (31) is a further confirmation of the consistency of both our picture of the granularity influence on  $S(T)$  and of the conditions given by Eqs. (31) and (40) to locate the MFR. Also, such an agreement seems to indicate that the use of  $\Delta L \approx 0$  in the MFR leads to qualitative but realistic relationships between  $S(T)$  and  $\sigma(T)$  [Eqs. (29) and (30)]. Concerning the MFR  $\epsilon$  limit, we may conclude here that the above-indicated analysis suggests that in  $\text{YBa}_2\text{Cu}_3\text{O}_{7-\delta}$  samples the MFR is located between  $\epsilon \approx 7 \times 10^{-3}$  and  $\epsilon \approx 0.13$ . These are the MFR  $\epsilon$  intervals indicated in various figures of this work.

## B. Background contributions and mean-field-like critical temperature

One of the basic and very general starting hypothesis of the theoretical approaches that we are going to use here to analyze our experimental results (see next subsection) is summarized by Eqs. (11), (12), and (25). In these equations, which are, in fact, the definitions of the ‘‘excess’’ of the corresponding magnitudes, it is explicitly assumed that above, but near, the transition each measured magnitude may be decomposed in two different contributions linearly additives. The first contribution, called ‘‘bare’’ or ‘‘background,’’ will arise from short-wavelength random fluctuations, and it is expected to be

rather insensitive to the presence of the transition. The other contribution is the so-called “excess,” and it will be due to the presence near the transition of long-wavelength fluctuations, with characteristic lengths of the order of the order-parameter correlation lengths. The theoretical treatments that we are going to use in the next subsection apply to the “excess” contribution of each transport coefficient. As a consequence, a meaningful comparison between the theories and the experimental results is possible only if the background part can be estimated *independently*,<sup>57</sup> the existing theoretical formalisms being unable to allow for these short-wavelength fluctuations.<sup>58</sup>

The above paragraph attempts to outline how the background or bare terms arise in the theoretical treatments of the critical behavior around a phase transition, and how important a proper and independent estimation of such terms is in comparing theory with experiment. In doing that, the fundamental and general assumption used is that such a background remains finite at the critical point if it is finite elsewhere.<sup>57</sup> A quantitative estimation of the background terms needs, however, the help of other conjectures which will depend on each transport property studied. In the case of the three observables studied here,  $\sigma(T)$ ,  $S(T)$ , and  $L(T)$ , one looks for any functional form, provided or not by the theory of the normal state, that fits closely the normal-state temperature trend over a wide temperature region far away from the transition, and that extrapolates smoothly through the transition.<sup>58</sup> The particular details in obtaining the normal behavior of each magnitude have been described in the preceding section. In the case of  $\rho(T)$  or  $\rho_{ab}(T)$ , the corresponding backgrounds are the solid lines in Figs. 2(a), 2(b), 3(a), and 3(b). In the case of  $S(T)$ , the corresponding background are the solid lines in Figs. 4(a) and 4(b). We must also note here that usually the background choice is a source of uncertainty unless a functional form for the normal-state temperature dependence and amplitude is firmly established. However, to our knowledge, at present *there is no alternative* to the empirical procedure summarized here to obtain  $\sigma_B(T)$  and  $S_B(T)$  *independently* of the corresponding excess.<sup>59</sup> In addition, in the case of  $\sigma_{abB}(T)$ , the normal behavior of  $\sigma_{ab}(T)$  is very well fitted by Eq. (7) up to  $T \lesssim 400$  K.<sup>60</sup> So, the modification of the background estimated in the present work proposed in other works,<sup>7,42</sup> could lead to the unreasonable conclusion of the existence of quite appreciable OPF effects at even more than 300 K above the transition. Furthermore, as already stressed in previous works,<sup>9,49</sup> it is obvious that with a free background almost any theoretical excess may fit reasonably well the experimental data, in any  $\epsilon$  region. This will, therefore, prevent any discrimination between the different theoretical explanations of the rounding effects on  $\rho(T)$  near  $T_c$  in HTSC.

In the case of  $S(T)$ , as a further analysis of the influence of the background choice on  $\Delta S(T)$ , we represent in Fig. 12(b)  $\Delta S(\epsilon)/S_B(\epsilon)$ , corresponding to sample Y3, and obtained by using, as an example, three different backgrounds, as illustrated in Fig. 12 (a). These three backgrounds have been obtained using Eq. (10) but

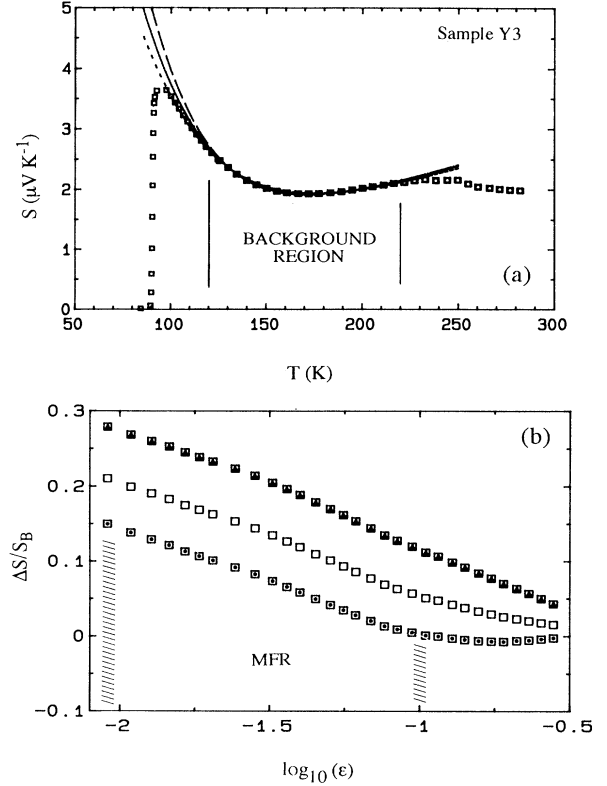


FIG. 12. An example of the influence of the background choice in the excess of  $S(T)$ . (a) Three backgrounds for sample Y3 corresponding to different  $b$  values in Eq. (10). The background temperature region of fitting is indicated. (b) Corresponding normalized excesses obtained from these backgrounds vs the logarithm of the reduced temperature. The mean-field region (MFR) is indicated. See main text for details.

with different values for  $b$  (with  $a$  and  $T_0$  as free parameters):  $b$  as free parameter (solid line), which leads to the values of Table II, and imposing  $b=100$  (short-dashed line), or imposing  $b=200$  (long-dashed line). The rms fit of these backgrounds between 120 and 220 K are, respectively, 3.5, 4.0, and 4.7%. Although the differences among these backgrounds are relatively important, their influence is manifest only on the  $\Delta S(\epsilon)$  amplitude, their  $\epsilon$  behavior remaining almost unchanged. We must note, however, that these changes of  $\Delta S(\epsilon)$  will change somewhat the  $\Delta L$  amplitude [in these examples,  $|\Delta L(\epsilon)/L_B(\epsilon)|$  will change by less than 0.1 over the entire MFR].

Let us finally recall that, as discussed in Refs. 8, 9, 12, and 13, we do not have a direct experimental access to  $T_{C0}$ , the mean-field-like critical temperature. However, it seems reasonable to expect that  $T_{C0}$  will be inside  $T_{CI} \pm \Delta T_{CI}$ , as defined before. This is also suggested by the fact that, in single-phase samples,  $T_{CX}$ , the temperature where the magnetic susceptibility goes through zero, is found to be within  $T_{CI} \pm \Delta T_{CI}$ .<sup>12,13</sup> Such an agreement has also been found here between  $T_{CI}$  and  $T_{CI}^S$  (see Tables I and II and Fig. 6), as was also noticed in Sec. III. So, in

the remainder of this paper we are going to approximate  $T_{C0}$  by  $T_{CI}$ .

### C. Comparison with the existing theoretical approaches in the mean-field region

We have seen before that our experimental results clearly suggest that all the OPF influence on  $S(T)$  arises through  $\sigma(T)$ . We will thus start the comparison of our experimental results with the available theoretical approaches for  $\Delta\sigma(\epsilon)$ . In previous works,<sup>8,9,12,13</sup> we have found that in the MFR the reduced-temperature behavior of  $\Delta\sigma(\epsilon)$  for different HTSC families is fairly well accounted for by the Lawrence-Doniach (LD) like extensions<sup>3,61–63</sup> to layered materials of the Aslamazov-Larkin results<sup>3,64</sup> for OPF effects on  $\rho(T)$  in isotropic superconductors. The LD model consists of superconducting planes separated by an effective distance,  $d_e$ , with a Josephson coupling between planes.<sup>61</sup> In zero applied magnetic field, it is reasonable to suppose that the fluctuations do not interact, so that each order-parameter component will have independent fluctuations which may be approximated as Gaussian. In this Gaussian approximation and independently of the type of pairing state or of the number,  $n$ , of real components of the order parameter<sup>61–63</sup>

$$\Delta\sigma_{ab}(\epsilon) = \frac{A_\sigma}{\epsilon} \left[ 1 + \frac{B}{\epsilon} \right]^{-1/2}, \quad (41)$$

where

$$B \equiv \left[ \frac{2\xi_c(0)}{d_e} \right]^2, \quad (42)$$

and where  $\xi_c(0)$  is the superconducting correlation length amplitude of the order parameter normal to the superconducting planes (in the  $c$  direction normal to the  $ab$  planes, in the case of the copper-oxide superconductors). In the original LD model,<sup>61</sup>  $d_e$  was the geometric distance between superconducting planes. However, in the most general situations (and, in particular, in the case of the copper-oxide superconductors, see later), inequivalent conducting layers at different distances may exist and the effective Josephson coupling between planes may be different. Therefore,  $d_e$  may differ from the geometric interplane distances, although it must be a sub-multiple of the unit-cell length,  $s$ , in the  $c$  direction.<sup>65</sup> This situation, together with the fact that pair-breaking effects could also contribute to  $\Delta\sigma(\epsilon)$ , has made it difficult to conclude on the precise  $d_e$  values.<sup>8,9</sup> However, recent measurements in different HTSC systems<sup>9</sup> and, mainly, measurements of the susceptibility rounding (not affected by pair-breaking effects) in the same HTSC compounds,<sup>12</sup> strongly suggest that in the case of YBCO samples  $d_e$  may be approximated as  $s$ . So, in the remainder part we will use  $s$  instead of  $d_e$ .

A crucial feature of Eq. (41) is that its amplitude parameter  $A_\sigma$  depends on the type of pairing state, on the number  $n$  of real components of the order parameter, and on the number  $N$  of conducting layers per unit-cell length,  $s$ . So,  $A_\sigma$  may be expressed as<sup>61–63,65</sup>

$$A_\sigma = gNA_{AL}, \quad (43)$$

where  $g$  is the number of complex components of the superconducting order parameter ( $g = n/2$ ),<sup>63,65</sup> and

$$A_{AL} = \frac{e^2}{16\hbar s} \quad (44)$$

is the Aslamazov-Larkin and Lawrence-Doniach universal conductivity. In the case of conventional  $^1s_0$ -wave pairing (one complex  $s$ -wave order parameter, i.e.,  $n=2$ ), or one complex-component unconventional pairing,  $g=1$ . Higher values of  $g$  would imply unconventional pairing (extended or non- $^1s_0$ -wave pairing). Other aspects of these approaches, as the possible influence on  $A_\sigma$  of the strength of the Josephson-like tunneling between layers, or the reduction of the  $A_\sigma$  value by the presence of impurities, may be seen in the original papers.<sup>61–65</sup> Note also that the original Lawrence-Doniach scenario<sup>61</sup> corresponds to conventional  $^1s_0$ -wave pairing ( $g=1$ , i.e.,  $n=2$ ), and to a single periodicity with one conducting layer per unit-cell length ( $N=1$ ).

In comparing Eq. (41) with our experimental results, we will start with those that directly correspond to the resistivity measurements. The solid lines in Figs. 3(b), 9(a), and 9(b) correspond to Eq. (41) with  $A_\sigma$  and  $B$  as free parameters. Note that Figs. 9(a) and 9(b) are, in fact, two different representation of the same  $\Delta\sigma(\epsilon)$  data, extracted from the  $\rho_{ab}(T)$  data of Fig. 3(b). The corresponding  $A_\sigma$  and  $B$  values are

$$A_\sigma = (350 \pm 100) \Omega^{-1} \text{cm}^{-1} \quad (45)$$

and

$$B = 0.15 \pm 0.08. \quad (46)$$

As expected, these values are, to within the experimental uncertainties, the same as we have obtained in previous measurements in granular samples,<sup>8,9,12</sup> by assuming  $d\rho_{abB}/dT \approx 0.5\mu\Omega \text{cm/K}$ . After the comments in Sec. III A, it is obvious that these values also agree with those obtainable from the  $\rho_{ab}(T)$  measurements in single-crystal samples<sup>6,7,42</sup> if  $\Delta\sigma_{ab}$  is extracted following the procedure indicated before in this work, or in previous references.<sup>8,9,12,13,49</sup> So, as also indicated before, the dramatic differences for  $\Delta\sigma_{ab}(\epsilon)$  among other works,<sup>42</sup> with one on one side and with our results on the other, are just due to discrepancies in the extraction of  $\Delta\sigma_{ab}(\epsilon)$  from the same  $\rho_{ab}(T)$  curve. Some of these differences have already been described in Ref. 9, and they are mainly associated with the arbitrary use, in some of these works, of a free background and a free mean-field critical temperature,  $T_{C0}$ .

A first conclusion of the above comparison is that *the  $\epsilon$  behavior* of the LD approach explains quite well our  $\Delta\sigma_{ab}(\epsilon)$  results over the entire MFR, the  $\epsilon$  region where this Gaussian approximation for OPF is expected to be applicable. Also, by using in Eq. (42),  $B = 0.15 \pm 0.08$  (and  $d_e \approx s = 11.7 \text{ \AA}$ ), we obtain  $\xi_c(0) \approx 2 \text{ \AA}$ , a value well inside the different proposals in the literature.<sup>51</sup> These values of  $B$ ,  $d_e$ , and  $\xi_c(0)$  were also found by Vidal *et al.* in analyzing both the *amplitude* and the  $\epsilon$  behavior of their paramagnetism measurements,<sup>12</sup> and they clearly

confirm the earlier paraconductivity-based proposals,<sup>8,9,12</sup> i.e., that OPF in these compounds are essentially 3D:  $\xi_c(\epsilon) > s$ , in most of the MFR. Note that this last result may be directly deduced from the fact that  $B$  is somewhat bigger than the high reduced-temperature limit of the MFR [see, e.g., Fig. 9(b)]. Note also that the fact that  $d_e$  may be approximated as  $s$  in the  $B$  expression seems to confirm that, as suggested before,<sup>42</sup> the Josephson coupling between the closest  $\text{CuO}_2$  planes (those separated by 3.4 Å) is strong enough to make them equivalent, from the point of view of the periodicity, to a unique layer of finite thickness (but with  $N=2$ ).

In what concerns the intrinsic  $\Delta\sigma_{ab}(\epsilon)$  amplitude, as we do not have access to the intrinsic  $\Delta S_{ab}(\epsilon)$  amplitude from our measurements in polycrystal samples, we are not going to analyze in detail our experimental  $\Delta\sigma_{ab}(\epsilon)$  results here. Let us note, however, that by using  $d_e \approx s = 11.7$  Å,  $N=1$ , and  $g=1$  in Eqs. (43) and (44), i.e., the original LD amplitude, we found  $A_\sigma \approx 130\Omega^{-1}\text{cm}^{-1}$ , which is less than half the value we found experimentally [Eq. (45)], confirming our previous findings.<sup>8,9,12</sup> [Let us recall here that if the intrinsic  $d\rho_{abB}/dT$  value in  $\text{YBa}_2\text{Ba}_2\text{Cu}_3\text{O}_{7-\delta}$  compounds would be of the order of  $1.4\mu\Omega\text{cmK}^{-1}$ , then by using Eq. (16) the amplitude deduced from the measurements would be  $A_\sigma \approx 130\Omega^{-1}\text{cm}^{-1}$ . However, all measurements in good single-crystal samples<sup>6,7,42</sup> suggest the value used here of  $0.5\mu\Omega\text{cmK}^{-1}$ .] This difference with the measured amplitude could be explained by the presence of a nonuniversal contributions to  $\Delta\sigma_{ab}(\epsilon)$  having the same  $\epsilon$  dependence in the MFR as the direct OPF contributions.<sup>12,13</sup> Such a contribution could be associated with pair-breaking (Maki-Thompson) effects, but then they should have a different  $\epsilon$  dependence than that proposed until now.<sup>54,66</sup> The two scenarios with  $g=1$  and  $N=2$ , or with  $g=2$  and  $N=1$  (always with  $d_e \approx s$ ), lead to  $A_\sigma \approx 260\Omega^{-1}\text{cm}^{-1}$ , which is compatible with our experimental values of  $A_\sigma$ . [Note also that a pair-breaking (Maki-Thompson) contribution to  $A_\sigma$  of the order of  $90\Omega^{-1}\text{cm}^{-1}$  will be acceptable, even with its conventional  $\epsilon$  dependence by the experimental  $B$  values.] In addition, through our previous data of the paradiamagnetism,  $\Delta\chi(\epsilon)$ , in the same samples<sup>12</sup> we found in this case  $\xi_{ab}(0) \approx 10$  Å. In previous analyses,<sup>12,13</sup> these two scenarios were discarded because this value of  $\xi_{ab}(0)$  was considered too low when compared with the published values.<sup>51</sup> However, recent analyses of the  $dH_{C2}(T)/dT$  measurements,<sup>67</sup> from which independent  $\xi_{ab}(0)$  values are obtained, seem to indicate that  $\xi_{ab}(0) \approx 10$  Å cannot be ruled out. In addition, with  $\xi_{ab}(0) \approx 10$  Å and  $\xi_c(0) \approx 2$  Å, from Eq. (32) we obtain  $\epsilon_G \approx 7 \times 10^{-3}$ , this last value being, as noted before, in excellent agreement with our experimental findings. So, concerning the  $\Delta\sigma_{ab}(\epsilon)$  amplitude, we may conclude here that the scenario with  $g=1$  (i.e., conventional  $^1s_0$  wave pairing or one complex-component unconventional pairing),  $d_e = 11.7$  Å, and  $N=2$  (i.e., two layers per unit-cell length in the  $c$  direction), seems to be compatible not only with our measurements, but also with the existing values for the characteristic Ginzburg-Landau lengths,  $\xi_{ab}(0)$  and  $\xi_c(0)$ , and that without the need, to within the exper-

imental uncertainties of  $\pm 100\Omega^{-1}\text{cm}^{-1}$ , of any nonuniversal contributions to  $\Delta\sigma_{ab}(\epsilon)$ . However, new precise independent data on  $\xi_{ab}(0)$  and  $\xi_c(0)$  will be very useful to confirm that possibility. Also,  $\Delta\sigma$  and  $\Delta\chi$  measurements in other copper-oxide systems with the same  $g$ , but with different values of  $N$ , will help to conclude about the other possible scenarios.

Coming back now to the results on the  $\epsilon$  behavior of  $\Delta\sigma(\epsilon)$ , they directly apply to  $\Delta S(\epsilon)$  through Eq. (27). This is shown in Figs. 10(a)–10(c), where  $(\sigma/\sigma_B)[\Delta S(\epsilon)/S_B(\epsilon)]$  is compared with  $\Delta\sigma(\epsilon)/\sigma_B(\epsilon)$ . The data points are the measurements. The solid line has been obtained from Eq. (16), with  $\Delta\sigma_{ab}(\epsilon)$  given by the Lawrence-Doniach expression [Eq. (41)] but by imposing the values of  $A_\sigma$  and  $B$  found before [Eqs. (45) and (46)]. As expected, the agreement between the experimental  $\Delta\sigma(\epsilon)/\sigma_B(\epsilon)$  and the theory is excellent. These results fully confirm our conclusions presented in Sec. IV B concerning the fact that  $\Delta L(\epsilon) \approx 0$  over the entire MFR and that the critical behavior of  $S(\epsilon)$  is driven by that of  $\sigma(\epsilon)$ .

We are now able to compare our data for  $\Delta L(\epsilon)$  with the available theory.<sup>2,68</sup> Unfortunately, the existing theoretical approaches for  $\Delta L(\epsilon)$  in the MFR mainly focus on its reduced-temperature behavior and a tractable estimate of its amplitude has not been published yet, although it is recognized that it must probably be very small,<sup>2,68</sup> in full agreement with our experimental findings presented here and in previous papers.<sup>18,19</sup> As a consequence, it is clear that nearly any functional form for  $\Delta L(\epsilon)$  can fit the data if a small enough amplitude is used. In spite of these difficulties, we compare in Fig. 13 our experimental data for  $\Delta L(\epsilon)$  with the theoretical expression proposed by Maki for  $s$ -wave layered superconductors in the clean limit,

$$\Delta L(\epsilon) = A_L \ln[2/\epsilon(1 + \alpha + \sqrt{1 + 2\alpha})], \quad (47)$$

where

$$\alpha \equiv B/2\epsilon \quad (48)$$

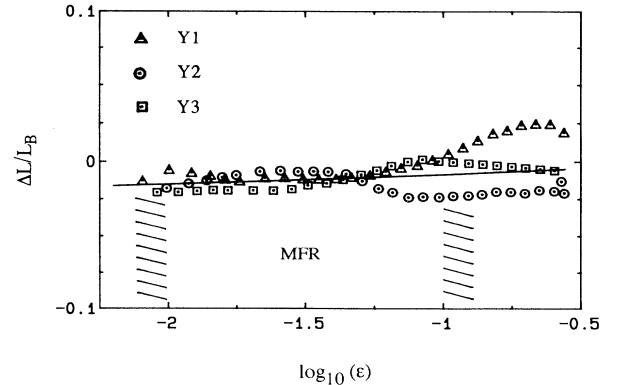


FIG. 13. Normalized excess of the thermoelectric coefficient vs the reduced temperature for the three samples used here. The solid line represents the best fit Maki's approach for layered superconductors.

and  $B$  is defined by Eq. (42). The amplitude  $A_L$  depends on  $T^3$ , on the electron-phonon coupling constant, and on the chemical potential. A somewhat disturbing feature of Eq. (47) is that its limit for  $\alpha \ll 1$  or  $\alpha \gg 1$  do not agree with previous calculations for films (2D) or bulk (3D) materials.<sup>2,53</sup> Although the latter cases were calculated in the dirty limit, the discrepancies remain even for the  $\epsilon$  dependence. In any case, the data points in Fig. 13 correspond to our experimental data of  $\Delta L(\epsilon)$  obtained for each of the three YBCO samples studied here, whereas the solid line has been obtained from Eq. (47), with  $B=0.15$ , and  $A_L$  as a free parameter. As noted above, the reasonable agreement between the theory and the data does not allow us to conclude about the adequacy of the  $\epsilon$  dependence of Eq. (47). In fact, this comparison allows us to only propose an upper limit to  $A_L$ , which is of the order of  $40 \mu\text{A}/\text{cm K}$ . This is, indeed, a very small amplitude, when compared with that of  $\sigma\Delta S(\epsilon)$  in the same  $\epsilon$  range, in agreement with the qualitative Maki suggestions.<sup>2,68</sup> A more detailed calculation of  $A_L$  in terms of more directly experimentally accessible parameters will allow a more quantitative comparison.

## VI. CONCLUSIONS

We have presented data of the thermoelectric power,  $S(T)$ , and of the electrical resistivity,  $\rho(T)$ , of three polycrystalline  $\text{YBa}_2\text{Cu}_3\text{O}_{7-\delta}$  samples, all with almost the same composition ( $\delta \lesssim 0.10$ ) and single phase to 4%, but with different granularity characteristics.  $S(T)$  and  $\rho(T)$  were measured in the temperature interval ranging from the superconducting transition to 300 K, the relative temperature resolution being 10 mK for  $\rho(T)$  and 50 mK for  $S(T)$ . Near the transition, the  $S(T)$  data are corrected from the influence of the nonzero temperature gradient ( $\nabla T \lesssim 1 \text{ K cm}^{-1}$ ) needed to perform the measurements. To take into account the influence on  $S(T)$  of the structural inhomogeneities (grains, crystallites, twinings) at long length scales, i.e., at length scales much larger than the superconducting correlation length in all directions, we have proposed an empirical picture, similar to that we have already used for  $\rho(T)$ , that explains fairly well the results for  $S(T)$  for the different granular samples studied here. From our experimental data we obtain the excess of the thermoelectric power,  $\Delta S(\epsilon)$ , and of the electrical conductivity,  $\Delta\sigma(\epsilon)$ , as a function of the reduced temperature,  $\epsilon$ , following a consistent procedure for both quantities. Our experimental data clearly indicate that in the so-called mean-field-like region, i.e., within  $\epsilon \approx 7 \times 10^{-3}$  to  $\epsilon \approx 0.15$ , the reduced-temperature

behavior of  $\Delta S(\epsilon)$  is not only very similar for the three different samples but also is very close to that of  $\Delta\sigma(\epsilon)$ . In contrast, the amplitudes of  $\Delta S(\epsilon)$  appreciably differ from sample to sample, although these differences remain much less important than for the  $\Delta\sigma(\epsilon)$  amplitudes. When analyzed in terms of the empirical picture proposed here for the influence on  $\Delta S(\epsilon)$  and  $\Delta\sigma(\epsilon)$  of the long length scale structural inhomogeneities, these results strongly suggest two important conclusions: (i) The observed  $\epsilon$  behavior of  $\Delta S(\epsilon)$  is similar to that of  $\Delta S_{ab}(\epsilon)$ , the intrinsic thermopower excess in the  $ab$  plane of an ideal single crystal of a similar composition to that of our granular samples. (ii)  $\Delta S_{ab}(\epsilon)$  and  $\Delta\sigma_{ab}(\epsilon)$  have, at a quantitative level, the same reduced-temperature behavior. In other words, all the influence of the order-parameter fluctuations on  $S(T)$  is driven by  $\sigma(T)$ : the thermoelectric power coefficient,  $L_{ab}(\epsilon)$ , connecting  $S_{ab}(\epsilon)$  with  $\sigma_{ab}(\epsilon)$ , will not be affected, in  $\text{YBa}_2\text{Cu}_3\text{O}_{7-\delta}$  superconductors, by order-parameter-fluctuation effects. These results have been compared with the existing theoretical approaches for the OPF effects on  $\sigma(T)$  and  $L(T)$  in layered superconductors, based on the OPF Gaussian approximation. The  $\epsilon$  dependence of both  $\Delta\sigma(\epsilon)$  and  $\Delta S(\epsilon)$  are fairly well accounted for by these theoretical approaches. The detailed comparison with  $\Delta L(\epsilon)$  is made difficult by the fact that  $\Delta L(\epsilon) \approx 0$ , this last result being also suggested, in fact, by these theoretical approaches. Although new measurements in good single-crystal samples will be very useful to confirm these results, we believe that the essential aspects of the OPF influence on the thermoelectric power in  $\text{YBa}_2\text{Cu}_3\text{O}_{7-\delta}$  samples are those presented in this work.

## ACKNOWLEDGMENTS

We acknowledge Y. P. Yadava and A. J. López for their substantial contributions to the design and construction of the apparatus used to measure  $S$ . We also thank E. Morán and co-workers and I. Rasines and co-workers for some of the samples, and V. L. Ginzburg and K. Maki for making available to us their results before publication. This work has been supported by the Comisión Interministerial de Ciencia y Tecnología Grant Nos. MAT 88-0769 and MAT 92-0841, the Programa Movilidad, Investigación, Desarrollo y Aplicaciones de los Superconductores Grant No. 89.3800, the Fundación Ramón Areces, and the Fundación Domingo Martínez, Spain.

<sup>1</sup>See, e.g., V. L. Ginzburg, *Physica C* **162-164**, 277 (1989); J. Supercond. **2**, 323 (1989); *Supercond. Sci. Technol.* **4**, S1 (1991), and references therein.

<sup>2</sup>K. Maki, *J. Low. Temp. Phys.* **14**, 419 (1974).

<sup>3</sup>See, e.g., W. J. Skocpol and M. Tinkham, *Rep. Prog. Phys.* **38**, 1049 (1975).

<sup>4</sup>P. P. Freitas, C. C. Tsuei, and T. S. Plaskett, *Phys. Rev. B* **36**, 833 (1987).

<sup>5</sup>M. Ausloos and Ch. Laurent, *Phys. Rev. B* **37**, 611 (1987).

<sup>6</sup>S. J. Hagen, T. W. Jing, Z. Z. Wang, J. R. Horvath, and N. P. Ong, *Phys. Rev. B* **37**, 7928 (1988).

<sup>7</sup>T. A. Friedman, M. W. Rabin, J. Giapintzakis, J. P. Rice, and D. M. Ginsberg, *Phys. Rev. B* **42**, 6217 (1990).

<sup>8</sup>J. A. Veira and F. Vidal, *Physica C* **159**, 468 (1989). Some other earlier references on the OPF effects on the electrical conductivity in YBCO compounds are given here.

- <sup>9</sup>J. A. Veira and F. Vidal, *Phys. Rev. B* **42**, 8748 (1990).
- <sup>10</sup>K. Kanoda, T. Takahashi, T. Kawagoe, T. Mizuguchi, M. Hasumi, and S. Kagoshima, *Physica C* **153-155**, 749 (1988); *J. Phys. Soc. Jpn.* **57**, 1554 (1988).
- <sup>11</sup>W. C. Lee, R. A. Klemm, and D. C. Johnston, *Phys. Rev. Lett.* **63**, 1012 (1989); W. C. Lee and D. C. Johnston, *Phys. Rev. B* **41**, 1904 (1990).
- <sup>12</sup>F. Vidal, C. Torrón, J. A. Veira, F. Miguez, and J. Maza, *J. Phys. Condens. Matter* **3**, 5219 (1991); **3**, 9257 (1991).
- <sup>13</sup>C. Torrón, O. Cabeza, J. A. Veira, J. Maza, and F. Vidal, *J. Phys. Condens. Matter* **4**, 4273 (1992).
- <sup>14</sup>H. J. Trodahl and A. Mawdsley, *Phys. Rev. B* **36**, 8881 (1987).
- <sup>15</sup>Ch. Laurent, S. K. Patapis, M. Laguesse, H. W. Vanderschueren, A. Rulmont, P. Tarte, and M. Ausloos, *Solid State Commun.* **66**, 445 (1988).
- <sup>16</sup>P. Clippe, Ch. Laurent, S. K. Patapis, and M. Ausloos, *Phys. Rev. B* **42**, 8611 (1990).
- <sup>17</sup>T. K. Dey, S. K. Ghatak, S. Srinivasan, D. Bhattacharya, and K. L. Chopra, *Solid State Commun.* **72**, 525 (1989); T. K. Dey, K. Radha, H. K. Barik, D. Bhattacharya, and K. L. Chopra, *ibid.* **74**, 1315 (1990).
- <sup>18</sup>O. Cabeza, Y. P. Yadava, J. Maza, C. Torrón, and F. Vidal, *Physica C* **185-189**, 1897 (1991).
- <sup>19</sup>O. Cabeza, J. A. Veira, J. Maza, Y. P. Yadava, F. Vidal, M. T. Casais, C. Cascales, and I. Rasines, in *Properties and Applications of Perovskite-Type Oxides*, edited by L. G. Tejuca and J. L. G. Fierro (Marcel Dekker, New York, 1992), Chap. 5, p. 101.
- <sup>20</sup>See, e. g., A. K. Bhatnagar, R. Pan, D. G. Naugle, G. R. Gilbert, and R. K. Pandey, *Phys. Rev. B* **41**, 4002 (1990); J. L. Cohn, E. F. Skelton, S. A. Wolf, and J. Z. Liu, *ibid.* **45**, 13 140 (1992).
- <sup>21</sup>C. Uher and A. B. Kaiser, *Phys. Rev. B* **36**, 5680 (1987).
- <sup>22</sup>M. A. Howson, M. B. Salamon, T. A. Friedman, S. E. Inderhees, J. P. Rice, D. M. Ginsberg, and K. M. Ghiron, *J. Phys. Condens. Matter* **1**, 465 (1989); M. A. Howson, M. B. Salamon, T. A. Friedman, J. P. Rice, and D. Ginsberg, *Phys. Rev. B* **41**, 300 (1990); A. J. Lowe, S. Regan, and M. A. Howson, *ibid.* **44**, 9757 (1991).
- <sup>23</sup>Z. Henkie, R. Horyn, Z. Bukowski, P. J. Markowski, and J. Klamut, *Solid State Commun.* **64**, 1285 (1987).
- <sup>24</sup>Ch. Laurent, S. K. Patapis, S. M. Green, H. L. Luo, C. Politis, K. Durczewski, and M. Ausloos, *Mode. Phys. Lett. B* **3**, 241 (1989).
- <sup>25</sup>A. J. Lopez, J. Maza, Y. P. Yadava, F. Vidal, F. García-Alvarado, E. Morán, and M. A. Señaris-Rodríguez, *Supercond. Sci. Technol.* **4**, S292 (1991).
- <sup>26</sup>Z. Z. Wang and N. P. Ong, *Phys. Rev. B* **38**, 7160 (1988).
- <sup>27</sup>M. Sera, S. Shamoto, and M. Sato, *Solid State Commun.* **68**, 649 (1988).
- <sup>28</sup>Lu Li, Ma Bei-Hai, Lin Shu-Yuan, Duan Hong-Min, and Zhang Dian-Lin, *Europhys. Lett.* **7**, 555 (1988).
- <sup>29</sup>A. B. Kaiser and G. Mountjoy, *Phys. Rev. B* **43**, 6266 (1991).
- <sup>30</sup>R. C. Yu, M. J. Naughton, X. Yan, P. M. Chaikin, F. Holtzberg, R. L. Greene, J. Stuart, and P. Davies, *Phys. Rev. B* **37**, 7963 (1988).
- <sup>31</sup>Lin Shu-Yuan, Lu Li, Duan Hong-Min, Ma Bei-Hai, and Zhang Dian-Lin, *Int. J. Mod. Phys. B* **3**, 409 (1989).
- <sup>32</sup>J. L. Cohn, S. A. Wolf, V. Selvanikov, and K. Salama, *Phys. Rev. Lett.* **66**, 1098 (1991), and references therein.
- <sup>33</sup>W. N. Kang, K. C. Cho, Y. M. Kim, and Mu-Yong Choi, *Phys. Rev. B* **39**, 2763 (1989).
- <sup>34</sup>J. P. Ouseph and M. Ray O'Bryan, *Phys. Rev. B* **41**, 4123 (1990).
- <sup>35</sup>C. Sulkowski, K. Rogacki, Z. Bukowski, R. Horyn, and E. Trojnar, *Physica C* **153-155**, 1337 (1988).
- <sup>36</sup>V. F. Gantmakher and D. V. Shovkun, *Pis'ma Zh. Eksp. Teor. Fiz.* **51**, 364 (1990) [*JETP Lett.* **51**, 413 (1990)].
- <sup>37</sup>J. Amador, C. Cascales, and I. Rasines, in *High-Temperature Superconductors*, edited by M. B. Brodsky, R. C. Dynes, K. Kitazawa, and H. L. Tuller, MRS Symposia Proceedings No. 99 (Materials Research Society, Pittsburgh, 1988), p. 249.
- <sup>38</sup>See, e.g., H. B. Callen, *Thermodynamics* (Wiley, New York, 1966), Chap. 17.
- <sup>39</sup>See, e.g., F. J. Blatt, P. A. Schroeder, C. L. Foiles, and D. Greig, *Thermoelectric Power of Metals* (Plenum, New York, 1976).
- <sup>40</sup>J. Maza and F. Vidal, *Phys. Rev. B* **43**, 10 560 (1991).
- <sup>41</sup>J. Kirtley, Y. Imry, and P. K. Hansman, *J. Low Temp. Phys.* **17**, 247 (1974).
- <sup>42</sup>M. Hikita and M. Suzuki, *Phys. Rev. B* **41**, 834 (1990); T. A. Friedman, J. P. Rice, J. Gianpirtzakis, and D. M. Ginsberg, *ibid.* **39**, 4258 (1989); K. Winzer and G. Kumm, *Z. Phys. B* **82**, 317 (1991); J. P. Rice, P. M. Giapintzakis, P. M. Ginsberg, and J. M. Mochel, *Phys. Rev. B* **44**, 10 158 (1991).
- <sup>43</sup>L. H. Greene and B. G. Bagley, in *Physical Properties of High-Temperature Superconductors II*, edited by D. M. Ginsberg (World Scientific, Singapore, 1990), Chap. 8.
- <sup>44</sup>P. W. Anderson and Z. Zou, *Phys. Rev. Lett.* **60**, 132 (1988).
- <sup>45</sup>See, e.g., F. Vidal, *Phys. Rev. B* **26**, 3986 (1982), and references therein.
- <sup>46</sup>M. Ausloos, K. Durczewski, S. K. Patapis, Ch. Laurent, and H. W. Vanderschueren, *Solid State Commun.* **65**, 365 (1988).
- <sup>47</sup>R. Srinivasan, V. Sandaranarayan, N. P. Raju, S. Natarajan, U. V. Varadaju, and G. V. Subba Rao, *Pranama J. Phys.* **29**, L225 (1987); C. D. Mukherjee, R. Ranganathan, A. K. Raychandhuri, and N. Chatterjee, *Phys. Status Solidi B* **154**, K55 (1989); V. Radharkrishnan, C. K. Subramanian, V. Sankaranarayanan, G. V. Subba Rao, and R. Srinivasan, *Phys. Rev. B* **40**, 6850 (1989).
- <sup>48</sup>F. Vidal, J. A. Veira, J. Maza, F. Miguez, E. Morán, and M. A. Alario, *Solid State Commun.* **66**, 421 (1988).
- <sup>49</sup>J. A. Veira, C. Torrón, J. Maza, and F. Vidal, *Physica B* **165-166**, 1367 (1990).
- <sup>50</sup>See, e.g., N. L. Bulaevskii, V. L. Ginzburg, and A. A. Sobyannin, *Physica C* **152**, 378 (1988).
- <sup>51</sup>See, e.g., B. Batlogg, *Physica B* **169**, 7 (1991).
- <sup>52</sup>See, e.g., E. Bonjour, R. Calemcuzuk, J. Y. Henry, and F. Khoder, *Phys. Rev. B* **43**, 106 (1991).
- <sup>53</sup>A. T. Dorsey, *Phys. Rev. B* **43**, 7575 (1991); S. Ullah and A. T. Dorsey, *ibid.* **44**, 262 (1991).
- <sup>54</sup>J. B. Bieri, K. Maki, and R. S. Thompson, *Phys. Rev. B* **44**, 4709 (1991).
- <sup>55</sup>N. L. Bulaevskii and I. D. Vager, *Phys. Rev.* **43**, 106 (1991).
- <sup>56</sup>J. A. Veira, J. Maza, and F. Vidal, *Phys. Lett. A* **131**, 310 (1988).
- <sup>57</sup>See, e. g., K. G. Wilson and J. Kogut, *Phys. Rep. C* **12**, 75 (1974).
- <sup>58</sup>See, e.g., F. Vidal, in *Macroscopic Theories on Superfluids*, edited by G. Grioly (Cambridge University Press, Cambridge, England, 1991), p. 95, and references therein.
- <sup>59</sup>Some authors [see, e.g., M. Hikita and M. Suzuki, *Phys. Rev. B* **39**, 4756 (1989); K. Semba, T. Ishii, and A. Matsuda, *Phys. Rev. Lett.* **67**, 769 (1991)] claim to avoid the uncertainties associated with the background by studying the magnetoconductivity and analyzing  $\Delta\bar{\sigma}(T,H)\equiv\sigma(T,H)-\sigma(T,0)$ , instead of  $\Delta\sigma(T,H)\equiv\sigma(T,H)-\sigma_B(T,H)$ . However, the existing theoretical approaches (see, e.g. Refs. 53, 54, and 66) are able

to calculate only the  $H$  influence on the OPF effects on  $\sigma(T, H)$ , i.e., they calculate  $\Delta\tilde{\sigma}(T, H) \equiv \Delta\sigma(T, H) - \Delta\sigma(T, 0)$ . It should thus be obvious that the comparison of the measured  $\Delta\tilde{\sigma}(T, H)$ , with the calculated  $\Delta\tilde{\sigma}(T, H)$  requires that even through the transition the background magnetoconductivity be negligible, i.e.,  $\sigma_B(T, H) = \sigma_B(T, 0)$ , an approximation affected by similar difficulties as the estimation of  $\sigma_B(T, 0)$ . In addition, as  $\Delta\tilde{\sigma} \ll \Delta\sigma$ , the different existing uncertainties affect more severely  $\Delta\tilde{\sigma}$  than  $\Delta\sigma$ . Also, the presence of an applied magnetic field may introduce additional complications in the OPF analyses (see, e.g., Ref. 53).

- <sup>60</sup>B. Batlogg, in *Physica of High-Temperature Superconductors*, edited by S. Maekawa and M. Sato (Springer-Verlag, Berlin, 1992), p. 219.
- <sup>61</sup>W. E. Lawrence and S. Doniach, in *Proceedings of the Twelfth International Conference on Low-Temperature Physics, Kyoto, Japan, 1970*, edited by E. Kanda (Keigatu, Tokyo, 1971), p.

361.

- <sup>62</sup>R. A. Klemm, *Phys. Rev. B* **41**, 2073 (1990).
- <sup>63</sup>S. Yip, *J. Low Temp. Phys.* **81**, 129 (1990).
- <sup>64</sup>L. G. Aslamazov and H. I. Larkin, *Phys. Lett.* **26A**, 238 (1968).
- <sup>65</sup>See, e.g., J. F. Annett, N. Goldenfeld, and S. R. Renn, in *Physical Properties of High Temperature Superconductors II*, edited by D. M. Ginsberg (World Scientific, New Jersey, 1990), p. 571; (private communication).
- <sup>66</sup>A. G. Aronov, S. Hikami, and H. I. Larkin, *Phys. Rev. Lett.* **62**, 965 (1989); K. Maki and R. S. Thompson, *Phys. Rev. B* **39**, 2769 (1989); J. B. Bieri and K. Maki, *ibid.* **42**, 4854 (1990).
- <sup>67</sup>See, e.g., D. K. Finnemore, in *Phenomenology and Applications of High-Temperature Superconductors*, edited by K. S. Bedill, M. Inni, D. Meltzer, J. R. Schrieffer, and S. Doniach (Addison-Wesley, Reading, MA, 1992), p. 164.
- <sup>68</sup>K. Maki, *Phys. Rev. B* **43**, 1252 (1991); **43**, 13 685 (1991).